Open access • Posted Content • DOI:10.1101/2021.03.31.437922

Functional architecture of the aging brain — Source link

Roni Setton, Laetitia Mwilambwe-Tshilobo, Manesh Girn, Amber W. Lockrow ...+18 more authors

Institutions: Montreal Neurological Institute and Hospital, University College London, University of Toronto, Harvard University ...+7 more institutions

Published on: 31 Mar 2021 - bioRxiv (Cold Spring Harbor Laboratory)

Topics: Connectome and Aging brain

Title: Functional architecture of the aging brain

Authors: Roni Setton[1*], Laetitia Mwilambwe-Tshilobo[1*], Manesh Girn[1], Amber W. Lockrow[1], Giulia Baracchini[1], Alexander J. Lowe[2], Benjamin N. Cassidy[3], Jian Li[4,5], Wen-Ming Luh[6], Danilo Bzdok[1,7,8,9,10] Richard M. Leahy[11], Tian Ge[12], Daniel S. Margulies[13], Bratislav Misic[1,8], Boris C. Bernhardt[1,8], W. Dale Stevens[14], Felipe De Brigard[15,16], Prantik Kundu[17], Gary R. Turner[14] and R. Nathan Spreng[1,8,18,19]

Affiliations:
[1] Montreal Neurological Institute, Department of Neurology and Neurosurgery, McGill University, Montreal, QC, Canada
[2] Institute of Neurology, University College London
[3] Department of Psychiatry, University of Toronto, Toronto, ON, Canada
[4]Athinoula A. Martinos Center for Biomedical Imaging, Department of Radiology, Massachusetts General Hospital, Charlestown, MA, USA
[5] Department of Neurology, Massachusetts General Hospital, Boston, MA, USA
[6] National Institutes of Health, National Institute on Aging, Baltimore, MD, USA
[7] Department of Biomedical Engineering, McGill University, Montreal, QC, Canada
[8] McConnell Brain Imaging Centre, McGill University, Montreal, QC, Canada
[9] School of Computer Science, McGill University, Montreal, QC, Canada
[10] Mila – Quebec Artificial Intelligence Institute, Montreal, QC, Canada
[11] Department of Electrical Engineering-Systems, University of Southern California, Los Angeles, CA, USA
[12] Psychiatric and Neurodevelopmental Genetics Unit, Center for Genomic Medicine, Massachusetts General Hospital, Boston, MA, USA
[13] Integrative Neuroscience and Cognition Center (UMR 8002), Centre National de la Recherche Scientifique (CNRS) and Université de Paris, Paris, France
[14] Department of Psychology, York University, Toronto, ON, Canada
[15] Department of Philosophy, Duke University, Durham, NC, USA
[16] Department of Psychology and Neuroscience, Durham, NC, USA
[17] Icahn School of Medicine at Mount Sinai, New York, NY, USA
[18] Departments of Psychiatry and Psychology, McGill University, Montreal, QC, Canada
[19] Douglas Mental Health University Institute, Verdun, QC, Canada

[*] Equal contribution

Correspondence:
R. Nathan Spreng
Montreal Neurological Institute
3801 University St.
Montréal, QC, H3A 2B4, Canada
p. 514-398-7268
f: 514-398-8248
e. nathan.spreng@gmail.com

Abstract

The intrinsic functional connectome can reveal how a lifetime of learning and lived experience is represented in the functional architecture of the aging brain. We investigated whether network dedifferentiation, a hallmark of brain aging, reflects a global shift in network dynamics, or comprises network-specific changes that reflect the changing landscape of aging cognition. We implemented a novel multi-faceted strategy involving multi-echo fMRI acquisition and de-noising, individualized cortical parcellation, and multivariate (gradient and edge-level) functional connectivity methods. Twenty minutes of resting-state fMRI data and cognitive assessments were collected in younger (n=181) and older (n=120) adults. Dimensionality in the BOLD signal was lower for older adults, consistent with global network dedifferentiation. Functional connectivity gradients were largely age-invariant. In contrast, edge-level connectivity showed widespread changes with age, revealing discrete, network-specific dedifferentiation patterns. Visual and somatosensory regions were more integrated within the functional connectome; default and frontoparietal regions showed greater coupling; and the dorsal attention network was less differentiated from transmodal regions. Associations with cognition suggest that the formation and preservation of integrated, large-scale brain networks supports complex cognitive abilities. However, into older adulthood, the connectome is dominated by large-scale network disintegration, global dedifferentiation and network-specific dedifferentiation associated with age-related cognitive change.

Keywords

connectivity, gradients, parcellation, network neuroscience, multi-echo fMRI

Spontaneous oscillations in brain activity provide the basis for characterizing large-scale functional networks (Biswal et al., 2010; Fox and Raichle, 2007; Yeo et al., 2011). This intrinsic functional network architecture is determined by both genetic factors and experience-dependent neuroplastic changes occurring across timescales, from moments to decades (Stevens and Spreng, 2014). Studying these networks in older adulthood can yield important insights into cognitive aging, and how a lifetime of learning and lived experience is instantiated in the aging brain. Key organizational features of the aging connectome include reduced within and greater between network connectivity (Geerligs et al., 2015), consistent with a dedifferentiated network architecture (Wig, 2017). An outstanding question is whether network dedifferentiation with age conveys information about the trajectory of neurocognitive aging. There are two tenable hypotheses. First, network dedifferentiation may represent a non-specific, global shift in network dynamics. Such global shifts may result from systemic alterations in structural, neurophysiological or metabolic factors, associated with domain general patterns of cognitive change. Alternatively, distinct patterns of network dedifferentiation may reflect specific changes in cognitive abilities in later life (Spreng and Turner, 2019). However, distinguishing between these possibilities presents significant methodological and conceptual challenges. Overcoming persistent and pervasive methodological limitations confronting resting-state functional connectivity (RSFC) investigations is critically necessary to fully leverage the value of this imaging modality as an indicator of brain and cognitive health in older adulthood. Here we adopt an innovative and multi-faceted data acquisition and analysis protocol to interrogate the precise nature of network dedifferentiation in older adulthood, thereby providing a more comprehensive account of the intrinsic network organization of the aging brain. To differentiate global from network specific changes in the aging connectome, we implemented several methodological innovations, described briefly below.

First we utilized multi-echo fMRI (ME-fMRI) data acquisition and a multi-echo independent components analysis (ME-ICA) preprocessing pipeline (Kundu et al., 2017). Innovations in ME-fMRI data acquisition protocols, combined with a TE-dependence model of BOLD signal denoising using ME-ICA, enables one to reliably separate BOLD from non-BOLD (i.e. noise) signal into different components (Kundu et al., 2017). Isolating neural components is chief among the challenges confounding investigations of age differences in resting-state fMRI. ME-ICA processing eliminates distant-dependent motion confounds (Power et al., 2017) and the need for multiple confound regression, including the global signal (Spreng et al. 2019), while allowing for valid between-group comparisons of the full range of positive and negative RSFC values. Recent validation work demonstrated that ME-fMRI processed data provides excellent reliability and temporal signal-to-noise, sufficient for individual-subject precision mapping (Lynch et al., 2020; Lynch, Elbau, Liston, 2021).

The number of independent BOLD components in ME-fMRI signal, or BOLD dimensionality, declines from childhood to middle-adulthood (Kundu et al., 2018). This putatively reflects the integration of spatially-distributed brain regions into large-scale functional networks in early adult development (Kundu et al., 2018). For the first time, we examine whether this global pattern of network reorganization persists into older adulthood. The integrity of large scale networks is reduced with age, as within-network connectivity declines and between-network

connections increase (Betzel et al., 2014; Madden et al., 2020; Malagurski et al., 2020; Stumme et al., 2020; Zonneveld et al., 2019). We predict that BOLD dimensionality, as a proxy for global network dedifferentiation, will be significantly lower for older versus younger adults. Further, we predict that reduced BOLD dimensionality in young, reflecting network integration, will be associated with better performance in cognitive domains requiring fast, integrative, and flexible processing. In contrast, reduced BOLD dimensionality in older adulthood may reflect global network dedifferentiation and be associated with lower performance on complex cognitive tasks.

Next we examined whether dedifferentiation is detectable as shifts in specific network interactions across the connectome. Topographic specificity in network dedifferentiation and integration may serve as a more selective marker of age-related cognitive changes (Ng et al., 2016; Reick et al., 2016; Spreng et al., 2016; Turner and Spreng, 2015). To investigate this possibility we first assessed age differences in macroscale connectivity gradient architecture across the cortex (Huntenburg et al., 2018; Margulies et al., 2016; Paquola et al., 2019; Vos de Wael et al., 2020). Gradients identify transitions in regional connectivity patterns, and changes with age would signal large-scale reorganization in functional brain organization. One recent investigation reported age-differences in gradient connectivity patterns (i.e., eccentricity of the gradient manifold; Bethlehem et al., 2020). However, only weak associations with cognition were reported. While little prior evidence is available, and none using ME-fMRI, gradients are robust, phylogenetic features of brain organization (Margulies et al., 2016). Thus we predict that these patterns would be resistant to normative ontogenetic changes. However, changes may emerge for regional connectivity profiles within the macroscale gradient architecture, reflecting network or node specific shifts in connectivity patterns.

To further evaluate this prediction of topographical specificity in network dedifferentiation, we conducted edge-level analyses using multivariate partial least squares analyses (PLS, Krishnan et al., 2011; McIntosh and Misic, 2013). This approach offers node and edge-level precision to detect age differences in the organization of functional brain networks, and associations with cognition. PLS analyzes the full edge-level connectivity matrix in a single statistical step, eliminating the need for additional thresholding within an *a priori* defined network parcellation scheme. This offers two methodological advantages. First we are able to identify reliable age-differences across the full edge-level connectivity matrix. Second, individual differences in the expression of these network connectivity patterns can be associated with individual differences in cognitive performance. We first examined edge-level connectomics within a canonical seven-network solution (Yeo et al., 2011). Based on previous work showing significant age changes among dorsal attention, default and frontoparietal control networks (Grady et al., 2016; Spreng & Schacter, 2012; Sullivan et al., 2019), we also conducted an *a priori analysis* of the sub-network topography for these three networks, derived from the 17-network solution by Yeo and colleagues (2011).

For both the gradient and edge-level connectivity analyses, we adopted an individualized functional parcellation approach to identify person-specific functional network nodes (Chong et al., 2017). Valid comparison of RSFC between younger and older adults may be compromised when template registration is unable to account for the individual variability in functional organization of the cortex (Braga and Buckner, 2017; Chong et al., 2017; Gordon, et al. 2017; Kong et al., 2019; Kong et al., 2021; Laumann et al., 2015; Wang et al., 2015). Deriving

functionally-defined, person-specific cortical parcellations can account for differences at the level of the individual which may introduce systematic biases in between group comparisons. Adopting an individualized parcellation approach further ameliorates noise artifacts that can obscure small yet reliable group differences, and increases power to detect reliable brain and behavior associations (Kong et al., 2021).

Here we bring together these innovative methods to conduct a comprehensive investigation into the intrinsic functional architecture of the aging brain. First, we examine age differences in the dimensionality of the BOLD signal, a global measure of network differentiation. Next, we examine macroscale gradient architecture as well as edge-level changes in the aging connectome. Finally, we examine observed global, gradient, and edge-level changes in large-scale brain networks for associations with aging cognition. This integrated approach provides a multiscale investigation of the shifting functional architecture of brain and cognition in later life.

Results

We implemented a multifaceted data acquisition and analysis protocol in 181 younger (M_{age}=22.59y) and 120 older (M_{age}=68.63y) healthy adults (See Table 1 and Methods and Materials). Overall, predicted age-group differences in cognition were observed. Younger adults performed better on indices of episodic memory ($t(281)= 17.51$ $p < .001$; Cohen's $d = 2.11$), executive function ($t(281)= 12.67$, $p <.001$; Cohen's $d=1.52$), and processing speed ($t(281)= 15.03$, $p < .001$; Cohen's $d = 1.81$). Older adults had higher semantic memory index scores ($t(281)= 9.18$, $p < .001$; Cohen's $d = 1.10$; see Table 1 for descriptives).

Table 1

Sample Demographics

	Younger Adults	Older Adults
N		
Cornell	154 (86 female)	84 (47 female)
York	27 (17 female)	36 (18 female)
Age (years)		
Range	18-34	60-89
M	22.6	68.6
SD	3.3	6.4
Education (years)*		
Range	12-24	12-24
M	15.2	17.2
SD	1.9	2.9
Episodic Memory*		
Range	-1.75-1.59	-1.99-0.70
M	0.52	-0.71
SD	0.53	0.66
Semantic Memory*		
Range	-2.78-1.39	-1.29-1.91
M	-0.35	0.48
SD	0.77	0.71
Executive Function*		
Range	-1.15-1.80	-2.03-0.76
M	0.36	-0.48
SD	0.56	0.53
Processing Speed*		
Range	-2.26-3.05	-2.40-.050
M	0.57	-0.78
SD	0.86	0.56

Table 1 Note: Episodic Memory, Semantic Memory, and Executive Function are index scores. Processing Speed is a z-score on Symbol Digit Modalities Task, Oral. * significant group differences.

BOLD Dimensionality

Two 10-minute runs of resting-state ME-fMRI were collected. BOLD dimensionality, the number of independent BOLD components in ME-fMRI signal, was stable across runs ($r(299) = .79$, $p < .001$, [.75, .83]; Figure 1A). Younger adults showed greater BOLD dimensionality than older adults ($t(299)=15.38$, $p < .001$; Cohen's $d= 1.81$; Figure 1B). In the context of lifespan development, which included an additional sample aged 8-46 (Kundu et al., 2018), a power function provided a suitable fit between age and BOLD dimensionality ($R^2=.547$; Figure 1C).

BOLD dimensionality demonstrated significant relationships with cognition (Table 2). In older adults, higher BOLD dimensionality was associated with higher episodic memory scores ($r(118)= .251$, $p < .01$, [.08, .41]). In younger adults, BOLD dimensionality showed a positive trending relationship with semantic memory ($r(161)= .155$, $p = .048$, [.00, .30]), which did not survive Bonferroni correction. Overlapping confidence intervals indicated no group differences in cognitive associations with BOLD dimensionality. Across the entire cohort, controlling for age, greater BOLD dimensionality was related to higher semantic memory scores ($pr(281) =.158$, $p < .01$, [.04, .27]) and lower executive function scores ($pr(281)= -.177$, $p <. 005$, [-.29, -.06]).

Figure 1

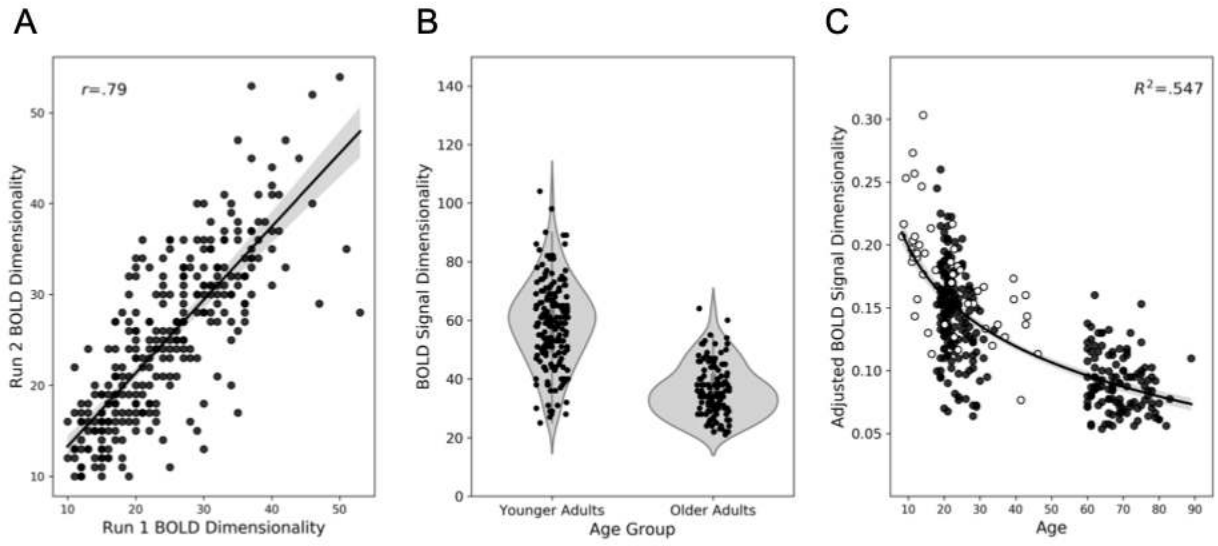

Figure 1 Caption: BOLD signal dimensionality (A) High test-retest reliability across two ME-fMRI runs. (B) Violin plots show distributions of total BOLD signal components across runs in younger and older adults. (C) The scatter plot shows BOLD signal dimensionality by age with a power distribution and 95% confidence intervals overlaid. Points in white were contributed by Kundu and colleagues (2018). Adjusted BOLD signal dimensionality = Total number of accepted BOLD components / number of time points acquired.

Gradients & Manifold Eccentricity

We next characterized gradients of functional connectivity in younger and older adults (e.g., Hong et al., 2019; Margulies et al., 2016). In both groups, the principal gradient spanned from unimodal regions to transmodal regions (Figure 2A). A whole-brain age group comparison revealed higher gradient values within bilateral superior parietal lobule in older adults (FWE $p <$ .05; cluster defining threshold $p <$ .01; Figure 2A). Here, higher gradient values represent greater functional connectivity similarity with transmodal regions as opposed to unimodal regions. In older adults, the superior parietal lobule is more closely affiliated with heteromodal cortex, including the default network, than in younger adults. The second gradient of cortical connectivity displayed a continuum of functional connectivity pattern similarity spanning visual cortex on one end to somatomotor and auditory cortices on the other (Figure 2B). Whole-brain group comparisons revealed no significant differences in the second gradient.

We rendered principal-second gradient manifold scatterplots in a 2D gradient embedding space in younger and older adults (Figure 2C). Older adults showed more diffuse and dedifferentiated vertices. We quantified this diffusivity by calculating manifold eccentricity –the sum of Euclidean distance across all vertices from the median– for each participant and compared across groups. Results revealed significantly greater manifold eccentricity in older adults ($t(299) = -10.74$, $p_{SPIN} < 0.01$, Cohen's d=1.26).

Manifold eccentricity associations with cognition were also examined (Table 2). In younger adults, manifold eccentricity was negatively related to episodic memory ($r(161) = -.191$, $p < .05$, [-.34, -.04]) and processing speed ($r(161) = -.168$, $p < .05$, [-.31, -.01]), but neither correlation survived Bonferroni correction. No relationships were observed in older adults, and no relationships remained across the full sample when controlling for age.

BOLD dimensionality and manifold eccentricity both demonstrated significant age-group differences. We conducted post-hoc product-moment correlations to test whether these global measures of brain organization were reliably associated. Negative correlations were observed in both younger ($r(179) = -.575$, $p < .001$, [-.64, -.50]) and older adults ($r(118) = -.255$, $p < .005$, [-.37, -.13]), such that higher BOLD dimensionality was related to less diffuse, more compact vertices in the manifold. In computing a partial correlation controlling for age, the relationship remained when performed on the full sample ($pr(299) = -.391$, $p < .001$, [-.48, -.29]). Non-overlapping 83% confidence intervals (Austin & Hux, 2002) indicated a significantly stronger correlation in younger adults.

Figure 2

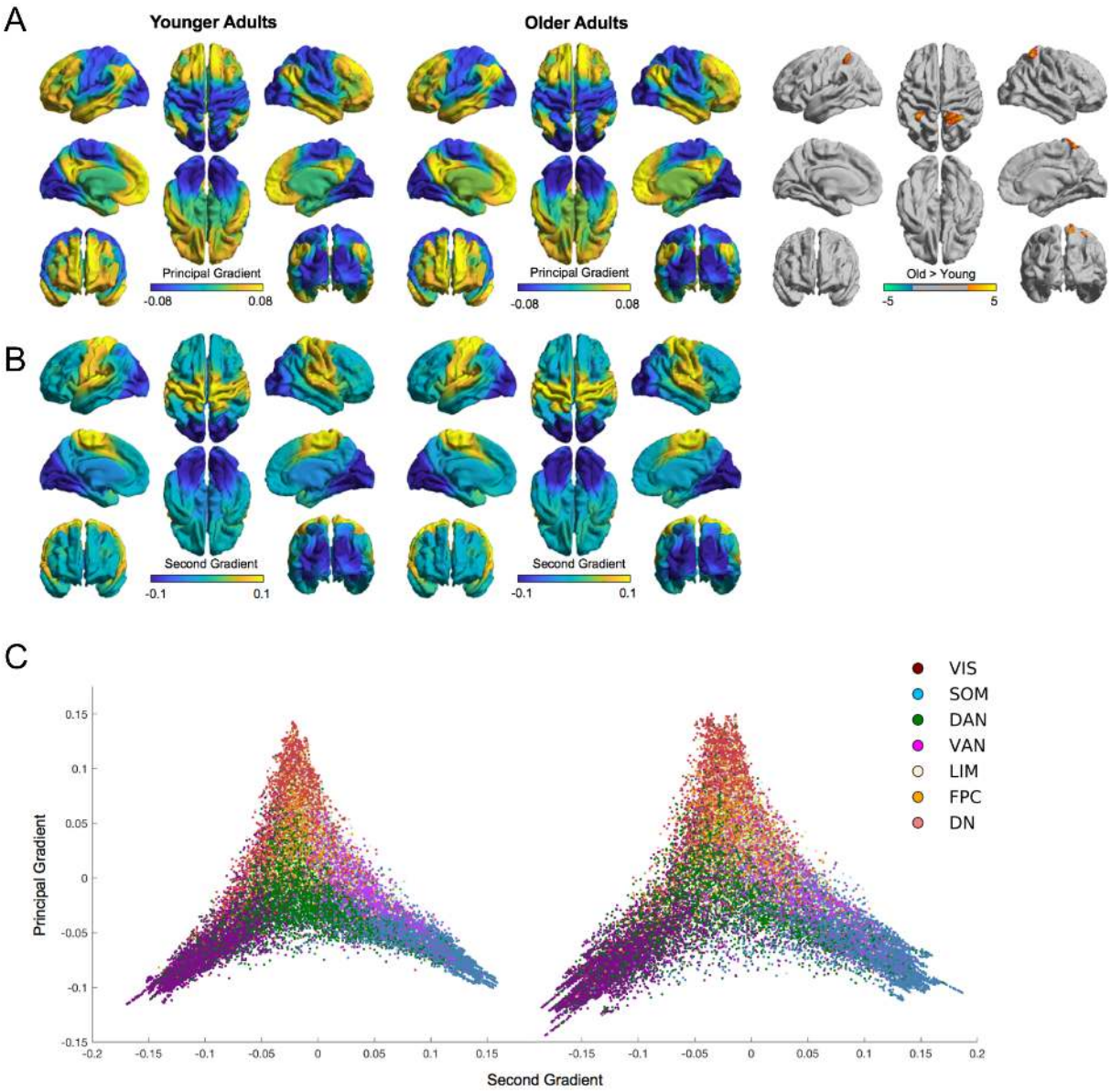

Figure 2 Caption: Gradients of cortical connectivity in younger and older adults. (A) The mean principal gradient for younger (left) and older (center) adults, representing an axis of functional connectivity similarity variance that ranged lowest to highest from unimodal to transmodal cortex. Older adults > younger adults contrast revealing statistically significant clusters at FWE $p < 0.05$, cluster defining threshold $p < 0.01$ (right). (B) The mean second gradient for younger (left) and older (right) adults, representing an axis of functional connectivity similarity variance that ranged lowest to highest from visual to somatomotor cortex. No group differences were observed for the second gradient. (C) Scatterplots representing the principal-second gradient manifold for younger (left) and older (right) adults. Scatterplot colors indicate functional network as per the 7-network solution by Yeo et al. (2011). VIS = visual, SOM= somatomotor, DAN= dorsal attention, VAN = ventral attention, LIM = limbic, FPC= frontoparietal control, DN= default.

Table 2: *BOLD Dimensionality and Manifold Eccentricity Correlations with Cognition*

Index	Younger Adults	Older Adults	Controlling for Age
BOLD Dimensionality			
Episodic Memory	.094 (.235)	**.251 (.006)***	.084 (.159)
Semantic Memory	.155 (.048)	.057 (.539)	**.158 (.008)***
Executive Function	-.146 (.062)	-.155 (.090)	**-.177 (.003)***
Processing Speed	.096 (.221)	-.018 (.848)	.016 (.784)
Manifold Eccentricity			
Episodic Memory	-.191 (.014)	-.073 (.430)	-.084 (.157)
Semantic Memory	-.134 (.088)	.020 (.832)	-.077(.196)
Executive Function	.040 (.609)	.094 (.305)	.085 (.154)
Processing Speed	-.168 (.032)	-.061 (.506)	-.080 (.182)

Table 2 Note: Within younger and older adults, r (*p*) values displayed. When controlling for age, pr (*p*) values displayed. * survives Bonferroni correction at $p < .013$.

Connectomics

We next examined whole-brain interregional functional connectivity differences between younger and older adults. Group mean connectivity matrices are in Figure 3A-B. Qualitative differences in the top 5% of positive connections between groups can be observed with a spring-embedded layout arranged by their network membership (Figure 3C-D). The spring-embedded plot displays stronger integration of the dorsal attention and frontoparietal control networks in older adults.

Age-related differences in the 79800 interregional connections (i.e., the lower triangle of the 400x400 functional connectivity matrix) were quantitatively assessed with PLS. A significant latent variable (permuted p = 0.0001) revealed a pattern of age differences in RSFC, with increases and decreases observed across the connectome (Figure 3E). Network contribution analysis of within- and between- network edges revealed significant age effects. Older adults demonstrated lower within-network connectivity across all seven networks, and lower connectivity between limbic, frontoparietal control and default networks (Figure 3F). Older adults showed greater between-network connectivity across systems for the visual and somatomotor networks (Figure 3G). The overall pattern of age-related differences was similar when examined with a 200 parcellation scheme (Supplementary Figure 3).

Brain connectivity scores were extracted from the group-wise difference in connectivity (Figure 3E) to interrogate how the observed pattern related to cognition. Higher brain connectivity scores for each age-group convey a stronger expression of the pattern of connectivity observed: greater within-network and lower between-network connectivity in younger adults; and lower within-network and greater between-network connectivity in older adults. Brain scores in younger adults were not reliably related to cognition, although a positive trending relationship with semantic memory was observed (r(161)= .158, p = .044, [.00, .30]; Table 3), which did not survive Bonferroni correction. Older adults' brain scores were negatively associated with executive function (r(118)= -.350, p < .001, [-.50, -.18]; Table 3). This indicates that greater between-network and lower within-network connectivity was negatively associated with executive function in older adults.

Figure 3.

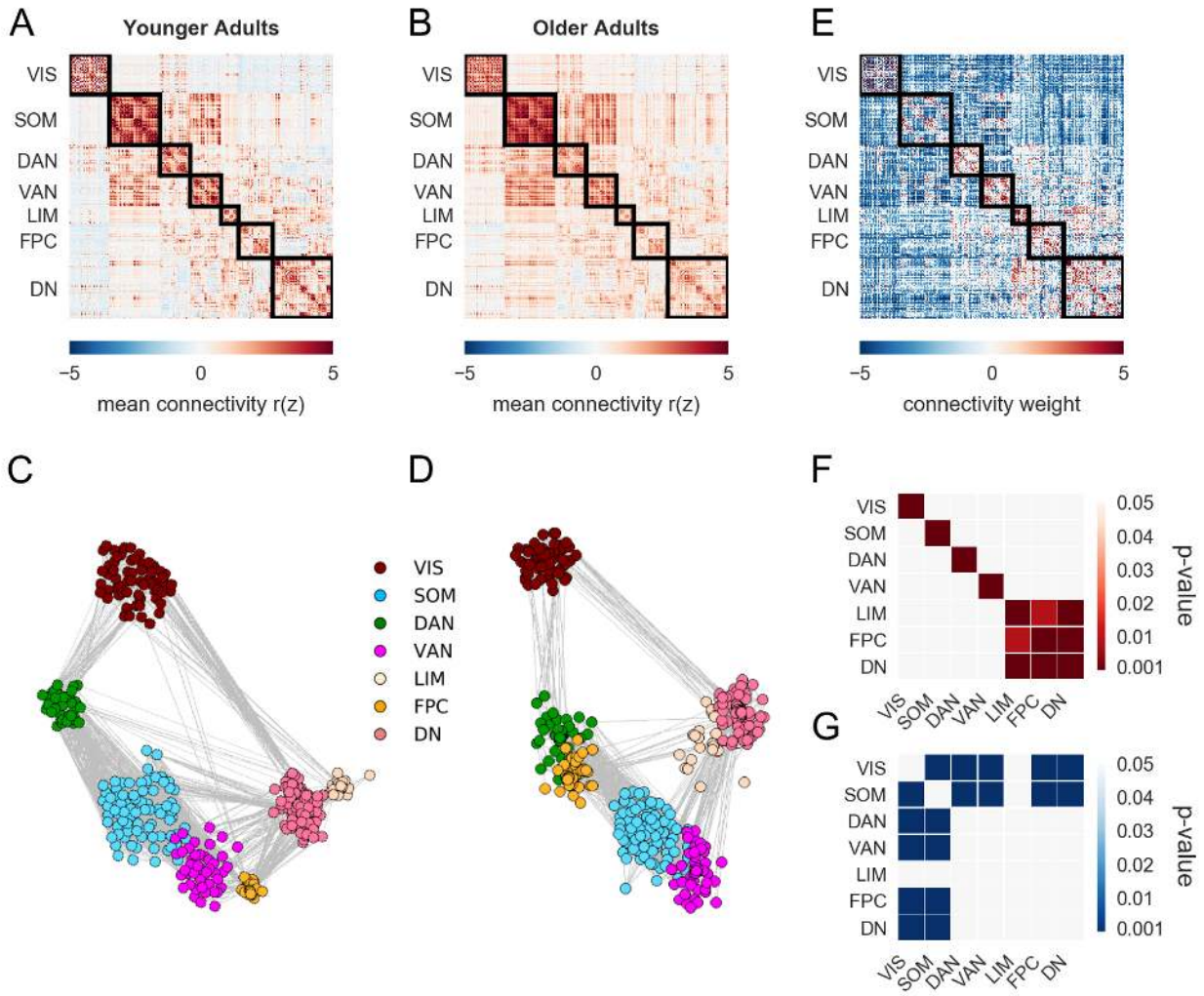

Figure 3 Caption: Functional connectomics in younger and older adults. Mean RSFC for the 400-parcellated data in (A) younger and (B) older adults. Spring-embedded plots with a 7-network solution (5% edge density) of the mean correlation matrices for (C) younger and (D) older adults. (E) Multivariate PLS analysis was used to identify age-related differences in RSFC between younger and older adults. Red color indicates significantly greater RSFC in younger adults, and blue color indicates significantly greater RSFC in older adults. (F-G) Network contributions reflecting differences in large-scale distributed networks. (F) Greater within- and between- network connectivity in younger adults. (G) Greater within- and between- network connectivity in older adults. The mean positive (F) and negative (G) bootstrap ratios within and between networks are expressed as a p-value for each z-score relative to a permuted null model. Higher z-scores indicate greater connectivity than predicted by the null distribution. VIS = visual, SOM= somatomotor, DAN= dorsal attention, VAN = ventral attention, LIM = limbic, FPC= frontoparietal control, DN= default.

Dorsal Attention, Frontoparietal Control, and Default Sub-Network Connectomics

In an *a priori*, targeted sub-network analysis we examined age-group differences in functional connectivity among subnetworks of the dorsal attention, frontoparietal control and default networks, and associations with cognition. The age-group average sub-network matrices are shown in Figure 4A-B. The spring-embedded representation of the average top 5% of positive connections in each group (Figure 4C-D) suggests that older adults show more integration of the default network (DN-A) and frontoparietal control network (CONT-A).

Quantitative comparison with PLS of the inter-regional functional connectivity revealed a distinct pattern of age differences (permuted $p < 0.001$; Figure 4E). Younger adults (Figure 4F) showed more within-network connectivity, and frontoparietal control to default connectivity (CONT-A to DN-A; CONT-A to DN-B; CONT-C to DN-C). Older adults (Figure 5G) showed greater between-network connectivity of the dorsal attention network (DAN-A) with all other sub-networks, as well as greater connectivity between the dorsal attention network (DAN-B) and the frontoparietal control (CONT-C) and default networks (DN-A). Older adults also showed greater connectivity between the frontoparietal control (CONT-C) and default network (DN-A). A similar pattern of connectivity was observed with a 200 parcellation scheme (Supplementary Figure 6).

Brain connectivity scores were extracted from the group-wise difference in dorsal attention, frontoparietal control and default sub-network connectomics (Figure 5E) and related to cognition. Sub-network brain connectivity scores did not show any reliable associations with cognition in younger adults (Table 3). In older adults, sub-network brain connectivity scores demonstrated a negative association with executive function ($r(118)= -.434$, $p < .001$, [-.57, -.28]; Table 3B).

Figure 4

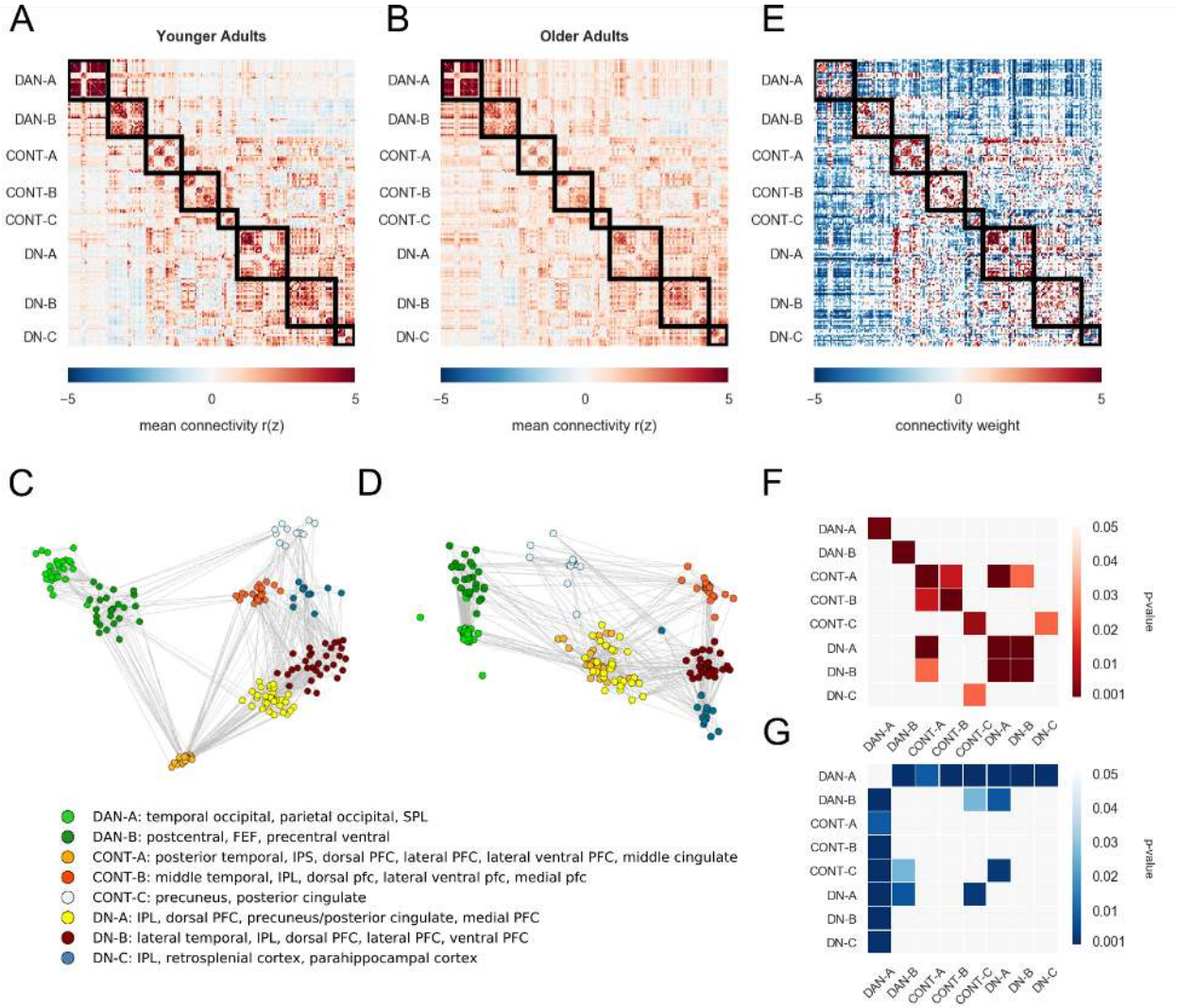

Figure 4 Caption: Functional connectivity of the dorsal attention (DAN), frontoparietal control (CONT), and default (DN) sub-networks following the Yeo 17-network solution. Mean group connectivity in (A) younger and (B) older adults. Spring-embedded plots (5% edge density) of the mean correlation matrices for (C) younger and (D) older adults. (E) Differences in RSFC between younger and older adults among DAN, CONT, and DN. (F) Greater within- and between- network connectivity in young. (G) Greater within- and between- network connectivity in older adults.

Table 3: *Composite Brain Connectivity Score Associations with Cognition*

Index	Younger Adults	Older Adults
Whole Brain		
Episodic Memory	.039 (.624)	.139 (.131)
Semantic Memory	.158 (.044)	-.001 (.993)
Executive Function	-.145 (.064)	**-.350 (.000)***
Processing Speed	.128 (.103)	-.062 (.504)
Sub-network		
Episodic Memory	.007 (.928)	.070 (.445)
Semantic Memory	.138 (.079)	.048 (.601)
Executive Function	-.126 (.109)	**-.434 (.000)***
Processing Speed	.128 (.102)	-.116 (.206)

Table 3 Note: r (*p*) values displayed. Subnetworks encompass the dorsal attention, frontoparietal control, and default networks. * survives Bonferroni correction.

Cross-Validation of the PLS Connectomics Findings

To verify that our results were not confounded by potential overfitting of the PLS model, the full and sub-network PLS analyses were conducted only on the first resting-state data run. Brain connectivity scores were then computed from the run one-derived weights and the run two individual-subject RSFC matrices and compared between groups. Age group differences were replicated in the held out run ($t(299)= 17.48$, $p < .001$, Cohen's $d= 2.06$). Additionally, brain connectivity scores derived from run two were significantly correlated with executive function in older adults ($r(118)= -.366$, $p < .001$, [-.51,-.20]). In the sub-network analysis, age group differences were also replicated in the held out run ($t(299)= 19.46$, $p < .001$, Cohen's $d= 2.29$). Sub-network brain connectivity scores derived from run two were also significantly correlated with executive function in older adults ($r(118)= -.425$, $p < .001$, [-.56,-.27]). These cross-validation analyses (see Supplementary Figure 7) demonstrate that the PLS results are robust to potential issues of model overfitting.

Discussion

These findings provide a comprehensive account of the intrinsic functional network architecture of the aging brain. Leveraging a novel multi-faceted strategy, we investigated whether network dedifferentiation, a hallmark of brain aging, reflects a global shift in network dynamics, or comprises network-specific changes that more closely adhere to the landscape of cognitive aging. Dimensionality, the number of BOLD components in the fMRI signal, was lower for older adults, consistent with a global pattern of network dedifferentiation. Macroscale connectivity gradients were age-invariant, suggesting that the macroscale functional architecture of the brain is largely preserved into older age. In contrast, edge-level connectivity analyses revealed three distinct network dedifferentiation patterns for older adults: Visual and somatomotor regions were more integrated within the broader connectome; default and frontoparietal regions showed greater coupling among the strongest edge-wise connections, and dorsal attention regions became less functionally segregated from other transmodal networks. These results provide the first multiscale analysis of age differences in the functional connectome. They reveal that the intrinsic network architecture of the aging brain is marked by both global and specific topographical patterns of network dedifferentiation. Associations with cognition suggest that the formation and preservation of integrated, large-scale brain networks can support complex cognitive abilities across the lifespan. However, in older adulthood the connectome becomes increasingly dominated by large scale network disintegration, global dedifferentiation and the emergence of network-specific connectivity patterns associated with age-related cognitive decline.

BOLD signal dimensionality and global network dedifferentiation

Dimensionality in the BOLD signal was significantly lower for older versus younger adults, reflecting a generalized pattern of network dedifferentiation continuing into later life. This finding builds upon an earlier report of cross-sectional dimensionality reductions from adolescence to early and middle adulthood (Kundu et al., 2018; Figure 1). Reductions in dimensionality in early adult development, largely attributable to functional integration among prefrontal and other transmodal cortices, reflects the transition from local connectivity to longer-range connections and the formation of spatially distributed yet intrinsically coherent brain networks (Kundu et al., 2018). The shift in functional brain organization parallels cognitive development over this period, which is marked by the emergence of more integrative and complex cognitive functions (Zelazo and Carlson, 2012), and is also evident within the structural connectome (Park et al., 2020). Our finding of an inverse relationship between dimensionality and executive functioning across the full sample, controlling for age, is consistent with this idea. Greater integration of distributed brain regions into stable yet discrete functional networks, indexed here by lower dimensionality, provides the neural substrate necessary to support complex cognitive abilities across the lifespan (Bullmore et al., 2009). Controlling for age, we also observed a positive association between BOLD signal dimensionality and semantic, or crystallized, knowledge. This correlation, driven largely by the younger group, is consistent with the shift from discrete, knowledge-dependent processing operations towards the emergence of more flexible, schema-based and integrative cognitive functions (Dumontheil, 2014; Ferrer et al., 2009). Within-group analyses revealed only a single positive correlation between dimensionality

and episodic memory in the older adult cohort. While speculative, this may reflect the integrity of the default network and its sub-network architecture in older adulthood (Andrews-Hanna et al., 2014). The medial temporal lobe subsystem, strongly implicated in episodic memory, is particularly vulnerable to age-related change (Buckner et al., 2005). The extent to which this subsystem is preserved as a distinct component of the default network, reflected as greater dimensionality in the BOLD signal, may support episodic memory performance into later life. Contrary to expectation, lower BOLD dimensionality was associated with higher executive functioning across the whole sample, discussed below.

Few studies have investigated BOLD signal dimensionality as a marker of adult cognitive development, and we are not aware of any published work investigating these associations in older adulthood. Our interpretations, therefore, of associations between dimensionality and cognitive abilities must be considered preliminary. What is clear from these findings is that the declines in the dimensionality of the BOLD signal, which begin in adolescence, continue unabated throughout adulthood and into later life. In younger adults, lower dimensionality reflects greater functional integration and the emergence of large-scale brain networks (Kundu et al., 2018). However, our observation of continued reductions in BOLD signal dimensionality into older adulthood suggests that network integration may reach an inflection point in middle age (Zonneveld et al., 2019). After this point, continued reductions in dimensionality may no longer be driven by network integration, but rather global network disintegration, and associated loss of coherent network components in the BOLD signal. While beyond the scope of the current report, such global shifts may result from systemic structural, neurophysiological, metabolic or cerebrovascular changes known to occur with advancing age (e.g., Tsvetanov et al., 2020).

Macroscale and edge-level connectomics

Reductions in BOLD signal dimensionality into older age suggests a global shift towards a dedifferentiated network architecture. We investigated whether this global shift may comprise more precise topographical patterns, reflected as integration between specific networks and nodes. We tested this hypothesis by examining both macroscale gradients and edge-level differences in the aging connectome. While this is the first report of gradient analyses using ME-fMRI and individualized parcellation methods, our findings largely recapitulate connectivity gradients observed in young adults (Margulies et al., 2016). Coherent transitions in functional connectivity patterns were observed from unimodal to transmodal association cortices (principal gradient) and from visual to somatomotor cortices (second gradient). The topography of both gradient patterns was preserved into older adulthood, indicating that the macroscale organization of cortical connectivity is largely age-invariant. We did observe closer alignment of the superior parietal lobule, a node of the dorsal attention network, with transmodal regions which include regions of the default network. This is consistent with earlier reports of reduced anticorrelation between the dorsal attention and default networks in later life (Spreng et al., 2016). As predicted, we did not find reliable associations between measures of gradient organization and cognition for either age group. While weak brain and behavior associations have been reported previously (Bethlehem et al., 2020), the current findings suggest that the macroscale gradient architecture of the brain is largely age-invariant and is likely an insensitive marker of age-related cognitive change.

To more precisely investigate edge-level connectivity patterns, we adopted a multivariate analytical approach. As PLS uses singular value decomposition to test age-differences across all edges in a single analytical step, we report RSFC differences across the full functional connectome, eliminating the need to apply functional connectivity strength or density thresholds. Visual inspection of the full connectomes for younger and older adults (Figure 3, Panels A-D) reveals a global pattern of network dedifferentiation for older adults, consistent with our dimensionality findings and previous reports (Betzel et al., 2014; Chan et al., 2014; Geerligs et al., 2015; Malagurski et al., 2020; Strumme et al., 2020). These qualitative differences were statistically validated in the group analysis (Figure 3, Panel E) and aggregate network matrices (Figure 3, Panels F-G). As predicted, younger adults showed a robust pattern of within-network connectivity, as well as connectivity between transmodal networks (Bullmore et al., 2009; Gratton et al., 2012).

Despite preserved macroscale gradients, edge-level analyses revealed striking age differences in network-specific connectivity patterns. First, within-network connectivity declined across the seven canonical networks investigated here. Reduced within-network functional connectivity is a hallmark of normative aging (Damoiseaux, 2017 for a review). As noted above, we speculate that degraded within-network coherence is likely a key determinant of reduced BOLD signal dimensionality in older adulthood. In addition to reduced within network coherence, edge-level analyses also revealed three distinct, network-specific dedifferentiation patterns. The most striking of these revealed greater integration of visual and somatomotor regions with all other networks for older adults (Figure 3, Panel G). Functional integration of visual and somatosensory regions has been observed previously. Age-related increases in node participation, a graph analytic marker of functional integration, were limited to visual and somatosensory networks in a large study of age-differences in RSFC (Geerligs et al., 2015). Connectivity patterns for visual regions showed greater alignment with other networks for older adults in a recent study of connectivity gradients (Bethlehem et al., 2020). Stumme and colleagues (2020) reported that age differences in RSFC were most prominent in visual and somatosensory cortices, and these changes mediated cognitive abilities in their older adult sample. Intrinsic functional integration of visual regions within the broader connectome is consistent with task-based evidence suggesting greater top-down modulation of visual association cortices by transmodal regions in older adulthood. Greater activation of transmodal cortices, in the context of age-related declines in the fidelity of sensory signaling, has been interpreted as increased demand for top-down modulation of early sensory processing (Clapp et al., 2011; Li and Rieckmann, 2014; Payer et al., 2006; Spreng and Turner, 2019). Indeed, sensory declines and motor slowing account for much of the individual variability in cognitive functioning among older adults (Baltes and Lindenberger, 1997; Salthouse, 1996). This suggests that greater modulation of these primary sensorimotor regions may be necessary to sustain complex thought and action in later life. While beyond the scope of the current study, we speculate that such task-driven demands for greater cross-talk between transmodal and sensorimotor cortices may, in turn, shape the intrinsic functional architecture of these networks in older adulthood.

We also conducted a targeted analysis of age-differences in the frontoparietal control, dorsal attention, and default networks. Previous work has demonstrated that these networks interact during goal-directed cognitive tasks (Spreng et al., 2010; Dixon et al., 2018; Murphy et al., 2020), show similar connectivity profiles during both task and rest (Spreng et al., 2013) and

undergo significant changes into older adulthood (Grady et al., 2016; Sullivan et al., 2019). For this *a priori* analysis, we adopted the sub-network topography for the three networks derived from the 17-network solution (Yeo et al., 2011). This enabled us to investigate age-related changes with greater precision. While the predicted pattern of reduced within-network connectivity was recapitulated across the sub-networks, two additional network-specific dedifferentiation patterns also emerged. As predicted, we observed greater age-related coupling of default and frontal brain regions, a pattern we have described as the Default to Executive Coupling Hypothesis of Aging (DECHA; Turner and Spreng, 2015; Spreng and Turner, 2019). This pattern did not emerge in the seven network analysis (Figure 3) or in the full, edge-level sub-network matrices (Figure 4, panels E-G). However, when we applied a connectivity threshold (top 5% of connectivity strengths), a clear DECHA pattern emerged for DN-A to Control-A sub-networks (Figure 3, panel C-D). We have posited that this dedifferentiation pattern may reflect the shifting architecture of cognition in later life (Spreng et al., 2018) with both adaptive and maladaptive consequences for cognitive aging (Spreng and Turner, 2019).

A second dedifferentiation pattern emerged in this sub-network analysis. Older adults showed greater connectivity between the dorsal attention and the two other association networks. This pattern was particularly pronounced for a DAN-A subnetwork which includes the superior parietal lobule. Previous reports have shown reduced anti-correlation between dorsal attention and default networks (Keller et al., 2015; Spreng et al., 2016) in older adulthood. These edge-level findings also converge with our gradient analyses where the superior parietal lobule, a core node of DAN-A, was the only region to show an age-difference in connectivity gradient, becoming more functionally integrated with other transmodal regions. The DAN-A sub-network encompasses regions of the frontal, parietal and temporal cortices implicated in top-down, or goal-directed, attentional control. This is again consistent with a neuromodulatory account of neurocognitive aging, wherein greater allocation of attentional resources may be engaged to sharpen perceptual representations in later life (Li et al., 2006; Li and Rieckmann, 2014).

BOLD dimensionality, functional connectivity and behavior

Our findings suggest that both global and network-specific dedifferentiation are core features of the functional aging connectome. In a final series of analyses we investigated whether these network changes were associated with aging cognition. Lower BOLD dimensionality, a marker of generalized network dedifferentiation, was associated with higher executive functioning across the whole sample, controlling for age. As noted above, this pattern has been associated with the formation of a more modular network architecture in early development (Kundu et al., 2018), and coincides with the emergence of executive control functions. Our data, the first to report dimensionality in older adults, suggests that the relationship between dimensionality and complex cognition may follow an inverted U-shaped function across the adult lifespan. In adolescence and early adulthood, decreasing dimensionality reflects an adaptive shift from discrete, localized processing units to a more integrated, large-scale, and lower dimensional network architecture, necessary to support complex cognitive functions across the adult lifespan. However, continued reductions in BOLD signal dimensionality into older age may reflect a transition from network integration to network dedifferentiation, and the (re)emergence of local processing networks. This interpretation is consistent with the recent observation that functional

network integration may reach an inflection point in middle adulthood, marking a shift from cognitive resilience to cognitive decline (Zonneveld et al., 2019).

This idea is consistent with reports associating network specific dedifferentiation with poorer functioning on standardized measures of complex cognition (Chan et al., 2014; Rieck et al., 2016; Spreng et al., 2018). We suggest that the emergence of these cross-network connections, in the context of global reductions in the integrity of canonical brain networks, represent the emergence of a more fractionated and maladaptive functional architecture into older age. We have also argued that the emergence of these age-specific, cross-network circuits (e.g., default to executive coupling) may also support or sustain complex, real world functioning in older adulthood (Spreng and Turner, 2019). However, testing this hypothesis will require more ecologically valid measures of complex cognition, and will be an important direction for future work.

Conclusion

Employing a multifaceted data acquisition and analysis protocol, we provide a comprehensive, multiscale account of the intrinsic functional architecture of the aging brain. As predicted, lower connectivity was observed within all canonical brain networks, and associated sub-networks, highlighting network dedifferentiation as a core feature of the aging connectome. Two distinct dedifferentiation patterns emerged from the analyses. Reduced BOLD signal dimensionality reflected the global shift towards a dedifferentiated network organization in older versus younger adults. While macroscale network organization was age invariant, edge-level analyses did reveal several network-specific patterns of dedifferentiation. Visual and somatomotor regions were more functionally integrated into the broader network connectome, default and frontoparietal control networks became more closely coupled, and the dorsal attention network showed less differentiation from other transmodal networks. Continued network dedifferentiation across the adult lifespan appears to reach an inflection point in later life, marking a shift from network integration to network dedifferentiation. This global shift in functional architecture is also accompanied by the emergence of specific cross-network connectivity patterns, likely marking the transition from an adaptive to a maladaptive network organization.

The methodological and analytical innovations implemented here ameliorated several of the most pervasive and enduring challenges in lifespan network neuroscience. These include age-related variability in noise profiles within the BOLD signal, as well as distortions introduced by group-wise spatial alignment to standardized templates. Of course, ME-fMRI protocols and individualized parcellations cannot address the totality of confounds that complicate cross-sectional data analyses. Among the most critical issues remaining involves resolving, or at least accurately modeling, age differences in neurovascular coupling. Altered neurovascular coupling with age can introduce spurious RSFC differences that are difficult to detect with standard imaging protocols (Tsvetanov et al., 2020). While ME-ICA methods, which separate neural from non-neural sources in the BOLD signal, are a significant advance, implementation of multimodal methods such as simultaneous arterial spin labeling and echo-planar imaging may be necessary to resolve this issue (Tsvetanov et al., 2020). Despite these limitations, we suggest that the methodological innovations implemented here provide a comprehensive, multi-faceted, and high-fidelity representation of age-differences in the functional network architecture of the brain.

Taken together, the findings add much needed clarity and precision to the current understanding of how functional networks are formed, shaped, and shifted into older adulthood.

Materials and Methods

Participants

Participants were 181 younger (M_{age}=22.59y, *SD*=3.27; 57% female) and 120 older (M_{age}=68.63y, *SD*=6.44; 54% female) healthy adults from Ithaca, New York, and Toronto, Canada (Table 1), rendering a total sample size of 301. Participants were screened to rule out individuals with a history of neurological or other medical illness known to impact cognition, acute or chronic psychiatric illness, those undergoing current or recent treatment with psychotropic medication, and those having experienced significant changes to health status within three months of the eligibility interview. Younger and older participants were screened for depressive symptoms using the Beck Depression Inventory (Beck et al., 1996) or the Geriatric Depression Scale (Yesavage et al., 1982), respectively. Two older adults were excluded due to a rating of "moderate depression". Older adults were additionally administered the Mini-Mental State Examination (MMSE; Folstein et al., 1975) to rule out mild cognitive impairment or sub-clinical dementia. Participants with MMSE scores below 27/30 were excluded if fluid cognition scores (Gershon et al., 2013) also fell below an age-adjusted national percentile of 25%. All participants were right-handed with normal or corrected-to-normal vision. Procedures were administered in compliance with the Institutional Review Board at Cornell University and the Research Ethics Board at York University.

Cognitive Assessment

283 of 301 individuals (163/181 younger adults, 120/120 older adults) underwent extensive cognitive assessment over three to four days prior to brain scanning. Index scores were created for cognitive domains of episodic memory, semantic memory, executive function, and processing speed (descriptives in Table 1). Episodic memory tasks included Verbal Paired Associates from the Wechsler Memory Scale-IV (Wechsler, 2009), the Associative Recall Paradigm (Brainerd et al., 2014), and NIH Cognition Toolbox Rey Auditory Verbal Learning and Picture Sequence Memory Tests (Gershon et al., 2013). Semantic memory tasks included Shipley-2 Vocabulary (Shipley et al., 2009), and NIH Cognition Toolbox Picture Vocabulary and Oral Reading Recognition Tests (Gershon et al., 2013). Executive function comprised the Trail Making Test (B-A; Reitan, 1958), the Reading Span Task (Daneman & Carpenter, 1980), NIH Cognition Toolbox Flanker Inhibitory Control and Attention task, Dimensional Change Card Sort, and List Sort Working Memory Tests (Gershon et al., 2013). Processing speed was tested with the Symbol Digit Modalities Test, Oral (Smith, 1982).

All data were z-scored. Index scores represent the average z-score (reversed where relevant) for all measures included within a cognitive domain. Across the four domains, higher scores represent better performance. Brain-behavior product-moment correlations were conducted at an alpha level of .05 with 83% confidence intervals (Austin & Hux, 2002) and Bonferroni adjustment for multiple comparison of $p<.013$ for four index score tests.

Neuroimaging

Image Acquisition

Imaging data were acquired on a 3T GE750 Discovery series MRI scanner with a 32-channel head coil at the Cornell Magnetic Resonance Imaging Facility or on a 3T Siemens Tim Trio MRI scanner with a 32-channel head coil at the York University Neuroimaging Center in Toronto. Scanning protocols were closely matched across sites. Anatomical scans at Cornell were acquired using a T1-weighted volumetric magnetization prepared rapid gradient echo sequence (TR=2530ms; TE=3.4ms; 7° flip angle; 1mm isotropic voxels, 176 slices, 5m25s) with 2x acceleration with sensitivity encoding. At York, anatomical scans were acquired using a T1-weighted volumetric magnetization prepared rapid gradient echo sequence (TR=1900ms; TE=2.52ms; 9° flip angle; 1mm isotropic voxels, 192 slices, 4m26s) with 2x acceleration and generalized auto calibrating partially parallel acquisition (GRAPPA) encoding at an iPAT acceleration factor of 2. Two 10m06s resting-state runs were acquired using a multi-echo (ME) EPI sequence at Cornell University (TR=3000ms; TE_1=13.7ms, TE_2=30ms, TE_3=47ms; 83° flip angle; matrix size=72x72; field of view (FOV)=210mm; 46 axial slices; 3mm isotropic voxels; 204 volumes, 2.5x acceleration with sensitivity encoding) and York University (TR=3000ms; TE_1=14ms, TE_2=29.96ms, TE_3=45.92ms; 83° flip angle; matrix size=64x64; FOV=216mm; 43 axial slices; 3.4x3.4x3mm voxels; 200 volumes, 3x acceleration and GRAPPA encoding). Participants were instructed to stay awake and lie still with their eyes open, breathing and blinking normally in the darkened scanner bay.

Image Processing

Anatomical images were skull stripped using the default parameters in FSL BET (Smith, 2002). Brain-extracted anatomical and functional images were submitted to ME-ICA (version 3.2 beta; https://github.com/ME-ICA/me-ica; Kundu et al., 2011; Kundu et al., 2013). ME-ICA relies on the TE-dependence model of BOLD signal to determine T2* in every voxel and separates BOLD signal from non-BOLD sources of noise. Prior to TE-dependent denoising, time series data were minimally preprocessed: the first 4 volumes were discarded, matrices were computed for de-obliquing, motion correction, and anatomical-functional coregistration, and volumes were brought into spatial alignment across TEs. The T2* maps were then used for anatomical-functional coregistration. Gray matter and cerebrospinal fluid compartments are more precisely delineated by the T2* map than by raw EPI images (Speck et al., 2001; Kundu et al., 2017), which is an important consideration in aging research where these boundaries are often blurred by enlarged ventricles and greater subarachnoid space. Volumes were then optimally combined across TEs and denoised.

Image quality assessment was performed on the denoised time series in native space to identify and exclude participants with unsuccessful coregistration, residual noise (in-scanner motion >3 mm coupled with denoised time series showing DVARS >1, Power et al., 2012), poor temporal signal to noise ratio < 50, or fewer than 10 retained BOLD-like components (see Supplementary Figure 1 for the group temporal signal to noise map).

The denoised BOLD component coefficient sets in native space, optimized for functional connectivity analyses (Kundu et al., 2013), were used in subsequent steps. We refer to these as multi-echo functional connectivity (MEFC) data. Additional measures were taken to account for

variation in the number of independent components from ME-ICA once connectivity matrices were estimated, as detailed below. MEFC neuroimages were mapped to a common cortical surface for each participant using FreeSurfer v6.0.1 (Fischl et al., 2012). To maximize alignment between intensity gradients of structural and functional data (Greve & Fischl, 2009), MEFC data were first linearly registered to the T1-weighted image by run. The inverse of this registration was used to project the T1-weighted image to native space and resample the MEFC data onto a cortical surface (fsaverage5) with trilinear volume-to-surface interpolation. Once on the surface, runs were concatenated and MEFC data at each vertex were normalized to zero mean and unit variance.

Individualized Parcellation. We generated participant-specific functional parcellations to examine individual differences in functional brain network organization using the Group Prior Individual Parcellation (GPIP; Chong et al., 2017). This approach enables a more accurate estimation of participant-specific individual functional areas (Chong et al., 2017) and is more sensitive to detecting RSFC associations with behavior (Kong et al., 2019; Mwilambwe-Tshilobo et al., 2019). The main advantage of this approach is that the correspondence among parcel labels is preserved across participants, while the parcel boundaries are allowed to shift based on the individual-specific functional network organization of each participant—thus providing a similar connectivity pattern that is shared across the population. Starting from an initial pre-defined group parcellation atlas, GPIP first refines each individual's parcel boundaries relative to their resting-state fMRI data. Next, the concentration (inverse covariance/partial correlation) matrices from all subjects are jointly estimated using a group sparsity constraint. GPIP iterates between these two steps to continuously update the parcel labels until convergence. Compared to other group-based parcellation approaches, GPIP has shown to improve the homogeneity of the BOLD signal within parcels and the delineation between regions of functional specialization (Chong et al., 2017).

We extracted MEFC data from each vertex and applied the above parcellation across the entire cohort of 301 participants at resolutions of 200 and 400 parcels. For each resolution, MEFC data were initialized to a group parcellation atlas developed by Schaefer et al. (2018). The two-step iterative process was repeated 20 times to produce a final parcellation representing the optimal partition with respect to the entire cortical surface. We calculated homogeneity by taking the average correlation coefficient of all pairs of vertices in a given parcel and then averaging across all parcels. This was repeated at each repetition to observe the incremental change in homogeneity as the iterative parcellation proceeded. Homogeneity was calculated first at the participant level and then averaged across the entire cohort for a group estimate. For a subset of participants, some parcels from the final partition merged into the medial wall (where no data existed) or into parcels belonging to the contralateral hemisphere. Because partitions likely reflect participant-specific neurobiological variations in functional organization, parcels assigned to the contralateral hemisphere were allowed to retain their original group atlas label. With the 400-parcel resolution, parcels merging with the medial wall occurred in 69 older adults and 35 younger adults, averaging 2-3 parcels in these participants; parcels migrating to the contralateral hemisphere occurred in 62 older adults and 24 younger adults, averaging 2-3 parcels. With the 200-parcel resolution, parcels merging with the medial wall occurred in 18 older adults and 10 younger adults, averaging 1 parcel in these participants. No parcels migrated to the contralateral hemisphere at this resolution.

Functional Connectivity Matrix. A connectivity matrix was constructed for each participant according to their individualized parcel solution. We extracted and spatially averaged the resulting MEFC data from each parcel and computed the product-moment correlation between each pair, resulting in a $n_{parcels} \times n_{parcels}$ functional connectivity matrix (Ge, Holmes, Buckner, Smoller, & Sabuncu, 2017). In this approach, RSFC was calculated as the correlation of the ICA coefficients across parcels, rather than a correlation across BOLD signal time-series, as is typically done (see Kundu et al., 2013). The canonical Fisher's r-to-z transformation was then applied to normalize the distribution of correlation values and account for variation in MEFC data degrees of freedom, or the number of de-noised ICA coefficients, across individuals (Kundu et al., 2013):

$$Z = \text{arctanh}(R) \cdot \sqrt{df - 3}$$

where R is the product-moment correlation value and *df* refers to the number of denoised ICA coefficients. Computing functional connectivity with approximately independent component coefficients rendered global signal regression unnecessary (Spreng et al., 2019). Critically, ME-ICA effectively removes distance-dependent RSFC motion confounds from fMRI data (Power et al., 2018).

Analysis

BOLD Dimensionality

A unique advantage of ME-fMRI and the ME-ICA processing framework is that BOLD- and non-BOLD-like signals can be separated into independent components. A novel metric of "BOLD dimensionality," the number of BOLD components identified in the ME-fMRI time series, may then be examined (e.g. Kundu et al., 2018). We assessed the test-retest reliability of BOLD dimensionality across two runs of data. Total BOLD dimensionality was then compared between groups with an independent samples *t*-test. To observe the trajectory of BOLD dimensionality with increasing age across the lifespan, BOLD dimensionality data from an independent developmental sample (N = 51, 10 female; M_{age}=21.9 years; age range, 8.3 – 46.2 years; see Kundu et al., 2018 for details) were pooled with the current data. To render the samples comparable and account for differences in acquisition across datasets, BOLD dimensionality was scaled by the number of timepoints acquired. The relationship between age and BOLD dimensionality was then fit to a power law function (see Supplementary Figure 2 for unscaled version).

Gradients & Manifold Eccentricity

Cortical gradients were computed using functions from the BrainSpace toolbox (https://github.com/MICA-MNI/BrainSpace; Vos de Wael et al., 2020), as implemented in MATLAB. For each participant, the 400 x 400 GPIP functional connectivity matrix was thresholded row-wise to the upper 10% of connections to retain only the strongest positive connections (Hong et al., 2019; Margulies et al., 2016). Cosine similarity was computed on the sparse matrix to input to the diffusion map embedding algorithm employed below, generating a matrix that captures similarity in whole-brain connectivity patterns between vertices (Hong et al., 2019; Margulies et al., 2016).

We then applied diffusion map embedding, a non-linear dimensionality manifold learning technique from the family of graph Laplacians (Coifman et al., 2005), to identify gradient components at the individual participant level. Each gradient represents a low-dimensional embedding estimated from a high-dimensional similarity matrix. In the embedding space, vertices that feature greater similarity in their whole-brain functional connectivity patterns appear closer together, whereas vertices that are dissimilar are farther apart. Each embedding axis can thus be interpreted as an axis of variance based on connectivity pattern similarity/dissimilarity. Euclidean distance in the embedded space is equivalent to the diffusion distance between probability distributions centered at those points, each of which is equivalent to a *difference in gradient* score. The algorithm is controlled by a single parameter α, which controls the influence of density of sampling points on the manifold with α = 0.5 (Margulies et al, 2016). This differentiates diffusion map embedding from Laplacian eigenmaps, and allows the inclusion of both global and local relationships in the estimation of the embedded space. An iterative Procrustes rotation was performed to align participant-specific gradient components to a Young-Old group average template and enable group comparisons. Group contrasts were conducted using surface-based linear models, as implemented in Surfstat (Worsley et al., 2009; http://www. math.mcgill.ca/keith/surfstat/).

We calculated a metric of manifold eccentricity to quantify the diffusivity of vertices in gradient space. Following Bethlehem et al. (2020) and Park et al. (2020), we summed the squared Euclidean distance of each vertex from the whole-brain median in a 2-dimensional gradient space for each participant. Mean manifold eccentricity was then compared across age groups. Statistical significance was determined with spin-test permutation testing, which overcomes biases in the test statistic due to the spatial autocorrelation inherent to BOLD data (Alexander-Bloch et al., 2018).

Edge-level Connectomics

Inter-regional functional connectivity group differences were determined with partial least squares (PLS). PLS is a multivariate method that determines the association between two sets of variables by identifying linear combinations of variables in both sets that maximally covary together (McIntosh and Lobaugh, 2004; McIntosh and Misic, 2013). In our analyses, one set of variables was individual RSFC matrices, while the other set represented group assignment or individual difference metrics.

Functional connectivity was assessed at the whole-brain level using the Schaefer atlas (Schaefer et al., 2018; Yeo et al., 2011; 400 x 400 matrix; 200 x 200 matrix as supplementary analysis, Supplementary Figure 3). Motivated by prior work (e.g., Grady et al., 2016; Sullivan et al., 2019; Spreng et al., 2016), we also examined RSFC among sub-networks of the default, frontoparietal control, and dorsal attention networks. For the sub-network analysis, we first reassigned each of the 400 parcels to the corresponding network of the Yeo 17-network solution following the mapping based on Schaefer et al. (2018). Next, we created a matrix for the pairwise connections between the following 8 sub-networks: dorsal attention (DAN-A, DAN-B), frontoparietal control (CONT-A, CONT-B, CONT-C), and default (DN-A, DN-B, DN-C) resulting in a 192x192 parcel matrix. The full 17-network characterization of the 400x400 parcel results, along with the 17-network and sub-network characterizations of the 200x200 matrix, can be found in Supplementary Figures 4, 5, and 7. At each level, a data matrix **X** was created using all

participants' parcellated functional connectivity matrices. The **X** matrix was organized such that each row corresponded to an observation (each participant, nested in age groups), and the cells in each column corresponded to the unique connections from each participant's connectivity matrix (the lower triangle of the matrix). The column means within each group were calculated, and the data in **X** were mean-centered. The mean-centered data were then submitted to singular value decomposition (SVD) to provide mutually orthogonal latent variables. Each latent variable represents a specific relationship (e.g. RSFC x Group) and consists of three elements: (1) a left singular vector consisting of the weighted connectivity pattern that optimally expresses the covariance, (2) a right singular vector, which represents the weights of the study design variables and can be interpreted as data-driven contrast weights between groups, and (3) a scalar singular value, which represents the covariance strength between the design variables (Group) and RSFC accounted for by each latent variable. Brain connectivity scores were calculated by taking the dot product of the left singular vector and each participant's RSFC matrix. A brain connectivity score, therefore, represents a single measure of the degree to which a participant expresses the connectivity pattern captured by a given latent variable.

All PLS latent variables were statistically evaluated using permutation testing. Rows of **X** were randomly reordered and subjected to SVD iteratively, as described above. This was done 1,000 times, creating a distribution of singular values under the null hypothesis of no existing relationships between X and Y for the corresponding PLS analysis, that there is no group difference in whole-brain (or sub-network) RSFC. A *p*-value was computed for each latent variable as the proportion of permuted singular values greater than or equal to the original singular value. Critically, permutation tests involve the entire multivariate pattern and are performed in a single analytic step, so correction for multiple comparisons is not required (McIntosh and Lobaugh, 2004).

Bootstrap resampling was used to estimate the reliability of weights for each RSFC edge. Participants were randomly resampled (rows in **X**) with replacement while respecting group membership. The matrix was subjected to SVD and the process was repeated 1,000 times, generating a sampling distribution for the weights in the singular vectors. To identify individual connections that made a statistically significant contribution to the overall connectivity pattern, we calculated the ratio between each weight in the singular vector and its bootstrap-estimated standard error. Bootstrap ratios are equivalent to z-scores if the bootstrap distribution is approximately unit normal (Efron and Tibshirani, 1986). Bootstrap ratios were, therefore, thresholded at values of ±1.96, corresponding to the 95% CI.

Network-Level Contributions

PLS analyses identified inter-regional connectivity patterns that differed by group and/or covaried with individual difference metrics. For each of these analyses, network-level effects were also examined. To quantify the network-level contributions to the PLS-derived functional connectivity pattern, two separate weighted adjacency matrices were constructed from positive and negative RSFC weights. For both matrices, nodes represent parcels defined by the individual parcellation, while edges correspond to the thresholded bootstrap ratio of each pairwise connection. Network-level functional connectivity contributions were quantified by assigning each parcel according to the network assignment reported by Yeo et al. (2011), and taking the average of all connection weights in a given network, thereby generating a 7 x 7 matrix (17 x 17

matrix for the 17-network solution; and an 8 x 8 matrix when examining interactivity for the default, frontoparietal control, and dorsal attention sub-networks). The significance of mean within- and between- network connectivity was computed by permutation testing. During each permutation, network labels for each node were randomly reordered and the mean within- and between- network connectivity were recalculated. This process was repeated 1000 times to generate an empirical null sampling distribution that indicates no relationship between network assignment and connectivity pattern (Shafiei et al., 2019). The significance of the pairwise connections of the original network matrix was determined by estimating the proportion of times the value of the sampling distribution was greater than or equal to the original value.

Spring-Embedded Plots

Spring-embedded plots were rendered from group average matrices of RSFC data using Pajek software (Mrvar & Batagelj, 2016). Sparse matrices containing the top 5% of positive connections were created and fed into Pajek. A partition was assigned based on the Yeo 7 or 17 network solution (Yeo et al., 2011) to optimize community (i.e., network) structure for visualization.

Acknowledgments

This work was supported in part by NIH Grant 1S10RR025145 and by a Canadian Institute of Health Research grant to R.N.S..

Competing Interests

The authors declare no competing interests.

References

Alexander-Bloch, A. F., Shou, H., Liu, S., Satterthwaite, T. D., Glahn, D. C., Shinohara, R. T., . Raznahan, A. (2018). On testing for spatial correspondence between maps of human brain structure and function. Neuroimage, 178, 540-551.

Andrews-Hanna, J. R., Smallwood, J., & Spreng, R. N. (2014). The default network and self-generated thought: Component processes, dynamic control, and clinical relevance. *Annals of the New York Academy of Sciences*, *1316*(1), 29–52. https://doi.org/10.1111/nyas.12360

Andrews-Hanna, J. R., Snyder, A. Z., Vincent, J. L., Lustig, C., Head, D., Raichle, M. E., & Buckner, R. L. (2007). Disruption of large-scale brain systems in advanced aging. *Neuron*, *56*(5), 924–935. https://doi.org/10.1016/j.neuron.2007.10.038

Austin, P. C., & Hux, J. E. (2002). A brief note on overlapping confidence intervals. *Journal of Vascular Surgery*, *36*(1), 194–195. https://doi.org/10.1067/mva.2002.125015

Beck, A.T., Steer, R.A., & Brown, G.K. (1996). Manual for the Beck Depression Inventory-II. San Antonio, TX: Psychological Corporation

Bethlehem, R. A. I., Paquola, C., Seidlitz, J., Ronan, L., Bernhardt, B., Consortium, C. C. A. N., & Tsvetanov, K. A. (2020). Dispersion of functional gradients across the adult lifespan. *NeuroImage*, *222*(July), 117299. https://doi.org/10.1016/j.neuroimage.2020.117299

Betzel, R. F., Byrge, L., He, Y., Goñi, J., Zuo, X. N., & Sporns, O. (2014). Changes in structural and functional connectivity among resting-state networks across the human lifespan. *NeuroImage*, *102 Pt 2*, 345–357. https://doi.org/10.1016/j.neuroimage.2014.07.067

Braga, R. M., & Buckner, R. L. (2017). Parallel Interdigitated Distributed Networks within the Individual Estimated by Intrinsic Functional Connectivity. *Neuron*, *95*(2), 457–471.e5. https://doi.org/10.1016/j.neuron.2017.06.038

Brainerd, C. J., Reyna, V. F., Gomes, C. F., Kenney, A. E., Gross, C. J., Taub, E. S., Spreng, R. N., & Alzheimer's Disease Neuroimaging Initiative (2014). Dual-retrieval models and neurocognitive impairment. *Journal of experimental psychology. Learning, memory, and cognition*, *40*(1), 41–65. https://doi.org/10.1037/a0034057

Buckner, R. L., Head, D., Parker, J., Fotenos, A. F., Marcus, D., Morris, J. C., & Snyder, A. Z. (2004). A unified approach for morphometric and functional data analysis in young, old, and demented adults using automated atlas-based head size normalization: Reliability and validation against manual measurement of total intracranial volume. *NeuroImage*, *23*(2), 724–738. https://doi.org/10.1016/j.neuroimage.2004.06.018

Buckner, R. L., Snyder, A. Z., Shannon, B. J., LaRossa, G., Sachs, R., Fotenos, A. F., … Mintun, M. A. (2005). Molecular, structural, and functional characterization of Alzheimer's disease:

Evidence for a relationship between default activity, amyloid, and memory. *Journal of Neuroscience*, *25*(34), 7709–7717. https://doi.org/10.1523/JNEUROSCI.2177-05.2005

Chan, M. Y., Park, D. C., Savalia, N. K., Petersen, S. E., & Wig, G. S. (2014). Decreased segregation of brain systems across the healthy adult lifespan. *Proceedings of the National Academy of Sciences of the United States of America*, *111*(46), E4997–E5006. https://doi.org/10.1073/pnas.1415122111

Chong, M., Bhushan, C., Joshi, A. A., Choi, S., Haldar, J. P., Shattuck, D. W., … Leahy, R. M. (2017). Individual parcellation of resting fMRI with a group functional connectivity prior. NeuroImage, 156(May), 87–100. https://doi.org/10.1016/j.neuroimage.2017.04.054

Clapp, W. C., Rubens, M. T., Sabharwal, J., & Gazzaley, A. (2011). Deficit in switching between functional brain networks underlies the impact of multitasking on working memory in older adults. *Proceedings of the National Academy of Sciences of the United States of America*, *108*(17), 7212–7217. https://doi.org/10.1073/pnas.1015297108

Coifman, R. R., Lafon, S., Lee, A. B., Maggioni, M., Nadler, B., Warner, F., & Zucker, S. W. (2005). Geometric diffusions as a tool for harmonic analysis and structure definition of data: Diffusion maps. Proceedings of the National Academy of Sciences of the United States of America, 102(21), 7426–7431. https://doi.org/10.1073/pnas.0500334102

Damoiseaux J. S. (2017). Effects of aging on functional and structural brain connectivity. *NeuroImage*, *160*, 32–40. https://doi.org/10.1016/j.neuroimage.2017.01.077

Daneman, M., & Carpenter, P. A. (1980). Individual differences in working memory and reading. *Journal of Verbal Learning and Verbal Behavior, 19*(4), 450. Retrieved from https://proxy.library.mcgill.ca/login?url=https://search.proquest.com/docview/1297349869?accountid=12339

Dixon, M.L., De La Vega, A., Mills, C. Andrews-Hanna, J.R., Spreng, R.N., Cole, M. & Christoff, K. (2018). Heterogeneity within the frontoparietal control network and its relationship to the default and dorsal attention networks. *Proceedings of the National Academy of Sciences USA*, 115(7), E1598–E1607. https://doi.org/10.1073/pnas.1715766115

Doucet, G. E., Labache, L., Thompson, P. M., Joliot, M., & Frangou, S. (2020). Atlas55+: Brain Functional Atlas of Resting-State Networks for Late Adulthood. *Cerebral Cortex*, 1–13. https://doi.org/10.1093/cercor/bhaa321

Dumontheil I. (2014). Development of abstract thinking during childhood and adolescence: the role of rostrolateral prefrontal cortex. *Developmental cognitive neuroscience*, *10*, 57–76. https://doi.org/10.1016/j.dcn.2014.07.009

Eickhoff, S. B., Yeo, B. T. T., & Genon, S. (2018). Imaging-based parcellations of the human brain. *Nature Reviews Neuroscience*, *19*(11), 672–686. https://doi.org/10.1038/s41583-018-0071-7

Efron, B., & Tibshirani, R. (1986). Bootstrap methods for standard errors, confidence intervals, and other measures of statistical accuracy. *Statistical Science*, *1*(1), 54–75. https://doi.org/10.1214/ss/1177013815

Felleman, D. J., & Van Essen, D. C. (1991). Distributed hierarchical processing in the primate cerebral cortex. *Cerebral cortex (New York, N.Y. : 1991)*, *1*(1), 1–47. https://doi.org/10.1093/cercor/1.1.1

Ferrer, E., O'Hare, E. D., & Bunge, S. A. (2009). Fluid reasoning and the developing brain. *Frontiers in Neuroscience*, *3*(MAY), 46–51. https://doi.org/10.3389/neuro.01.003.2009

Fox, M. D., & Raichle, M. E. (2007). Spontaneous fluctuations in brain activity observed with functional magnetic resonance imaging. *Nature Reviews. Neuroscience*, *8*(9), 700–711. https://doi.org/10.1038/nrn2201

Fischl, B. (2012). FreeSurfer. NeuroImage, 62(2), 774–781. https://doi.org/10.1016/j.neuroimage.2012.01.021

Folstein, M. F., Folstein, S. E., & McHugh, P. R. (1975). "Mini-Mental State" A practical method for grading the cognitive state of patients for the clinician. Journal of Psychiatric Research, 12, 189–198. http://doi.org/10.1016/0022-3956(75)90026-6

Ge, T., Holmes, A.J., Buckner, R.L., Smoller, J.W., Sabuncu, M.R. (2017). Heritability analysis with repeat measurements and its application to resting-state functional connectivity. Proceedings of the National Academy of Sciences, 114(21), 5521–6. https://doi.org/10.1073/pnas.1700765114.

Geerligs, L., Renken, R. J., Saliasi, E., Maurits, N. M., & Lorist, M. M. (2015). A brain-wide study of age-related changes in functional connectivity. *Cerebral Cortex*, *25*(7), 1987–1999. https://doi.org/10.1093/cercor/bhu012

Gershon, R. C., Wagster, M. V., Hendrie, H. C., Fox, N. A., Cook, K. F., & Nowinski, C. J. (2013). NIH toolbox for assessment of neurological and behavioral function. *Neurology*, *80*(11 Suppl 3), S2–S6. https://doi.org/10.1212/WNL.0b013e3182872e5f

Glover, G.H., Li, T.-Q. and Ress, D. (2000), Image-based method for retrospective correction of physiological motion effects in fMRI: RETROICOR. Magn. Reson. Med., 44: 162-167. https://doi.org/10.1002/1522-2594(200007)44:1.

Gotts, S. J., Gilmore, A. W., & Martin, A. (2020). Brain networks, dimensionality, and global signal averaging in resting-state fMRI: Hierarchical network structure results in low-dimensional spatiotemporal dynamics. *NeuroImage*, *205*, 116289. https://doi.org/10.1016/j.neuroimage.2019.116289

Gordon, E. M., Laumann, T. O., Adeyemo, B., Gilmore, A. W., Nelson, S. M., Dosenbach, N., & Petersen, S. E. (2017). Individual-specific features of brain systems identified with resting state functional correlations. *NeuroImage*, *146*, 918–939. https://doi.org/10.1016/j.neuroimage.2016.08.032

Grady, C., Sarraf, S., Saverino, C., & Campbell, K. (2016). Age differences in the functional interactions among the default, frontoparietal control, and dorsal attention networks. *Neurobiology of Aging*, *41*, 159–172. https://doi.org/10.1016/j.neurobiolaging.2016.02.020

Gratton, C., Nomura, E. M., Pérez, F., & D'Esposito, M. (2012). Focal brain lesions to critical locations cause widespread disruption of the modular organization of the brain. *Journal of cognitive neuroscience*, *24*(6), 1275–1285. https://doi.org/10.1162/jocn_a_00222

Greicius, M. D., Srivastava, G., Reiss, A. L., & Menon, V. (2004). Default-mode network activity distinguishes Alzheimer's disease from healthy aging: evidence from functional MRI. *Proceedings of the National Academy of Sciences of the United States of America*, *101*(13), 4637–4642. https://doi.org/10.1073/pnas.0308627101

Greve, D. N., & Fischl, B. (2009). Accurate and robust brain image alignment using boundary-based registration. NeuroImage, 48(1), 63–72. https://doi.org/10.1016/j.neuroimage.2009.06.060

Haxby, J. V., Guntupalli, J. S., Connolly, A. C., Halchenko, Y. O., Conroy, B. R., Gobbini, M. I., … Ramadge, P. J. (2011). A common, high-dimensional model of the representational space in human ventral temporal cortex. *Neuron*, *72*(2), 404–416. https://doi.org/10.1016/j.neuron.2011.08.026

Hong, S.-J., de Wael, R. V., Bethlehem, R. A., Lariviere, S., Paquola, C., Valk, S. L., . . . Smallwood, J. (2019). Atypical functional connectome hierarchy in autism. Nature communications, 10(1), 1022.

Jo, H. J., Saad, Z. S., Simmons, W. K., Milbury, L. A., & Cox, R. W. (2010). Mapping sources of correlation in resting state FMRI, with artifact detection and removal. *NeuroImage*, *52*(2), 571–582. https://doi.org/10.1016/j.neuroimage.2010.04.246

Kaas J. H. (1987). The organization of neocortex in mammals: implications for theories of brain function. *Annual review of psychology*, *38*, 129–151. https://doi.org/10.1146/annurev.ps.38.020187.001021

Keller, J. B., Hedden, T., Thompson, T. W., Anteraper, S. A., Gabrieli, J. D., & Whitfield-Gabrieli, S. (2015). Resting-state anticorrelations between medial and lateral prefrontal cortex: association with working memory, aging, and individual differences. *Cortex; a journal devoted to the study of the nervous system and behavior*, *64*, 271–280. https://doi.org/10.1016/j.cortex.2014.12.001

Kong, R., Li, J., Orban, C., Sabuncu, M. R., Liu, H., Schaefer, A., … Yeo, B. T. T. (2019). Spatial Topography of Individual-Specific Cortical Networks Predicts Human Cognition, Personality, and Emotion. Cerebral Cortex, 29(6), 2533–2551. https://doi.org/10.1093/cercor/bhy123

Krishnan, A., Williams, L. J., McIntosh, A. R., & Abdi, H. (2011). Partial Least Squares (PLS) methods for neuroimaging: a tutorial and review. *NeuroImage*, *56*(2), 455–475. https://doi.org/10.1016/j.neuroimage.2010.07.034

Kundu, P., Santin, M. D., Bandettini, P. a., Bullmore, E. T., & Petiet, A. (2011). Differentiating BOLD and non-BOLD signals in fMRI time series using multi-echo EPI. NeuroImage, 60, 1759–1770.

Kundu, P., Brenowitz, N. D., Voon, V., Worbe, Y., Vértes, P. E., Inati, S. J., … Bullmore, E. T. (2013). Integrated strategy for improving functional connectivity mapping using multiecho fMRI. Proceedings of the National Academy of Sciences of the Unites States of America, 110(40), 16187–16192. http://doi.org/10.1073/pnas.1301725110

Kundu, P., Voon, V., Balchandani, P., Lombardo, M. V., Poser, B. A., & Bandettini, P. A. (2017). Multi-echo fMRI: A review of applications in fMRI denoising and analysis of BOLD signals. NeuroImage, 154(March), 59–80. https://doi.org/10.1016/j.neuroimage.2017.03.033

Kundu, P., Benson, B. E., Rosen, D., Frangou, S., Leibenluft, E., Luh, W. M., … Ernst, M. (2018). The integration of functional brain activity from adolescence to adulthood. Journal of Neuroscience, 38(14), 3559–3570. https://doi.org/10.1523/JNEUROSCI.1864-17.2018

Laumann, T. O., Gordon, E. M., Adeyemo, B., Snyder, A. Z., Joo, S. J., Chen, M. Y., Gilmore, A. W., McDermott, K. B., Nelson, S. M., Dosenbach, N. U., Schlaggar, B. L., Mumford, J. A., Poldrack, R. A., & Petersen, S. E. (2015). Functional System and Areal Organization of a Highly Sampled Individual Human Brain. *Neuron*, *87*(3), 657–670. https://doi.org/10.1016/j.neuron.2015.06.037

Li, J., Kong, R., Liégeois, R., Orban, C., Tan, Y., Sun, N., Holmes, A. J., Sabuncu, M. R., Ge, T., & Yeo, B. (2019). Global signal regression strengthens association between resting-state functional connectivity and behavior. *NeuroImage*, *196*, 126–141. https://doi.org/10.1016/j.neuroimage.2019.04.016

Li, S. C., & Rieckmann, A. (2014). Neuromodulation and aging: implications of aging neuronal gain control on cognition. *Current opinion in neurobiology*, *29*, 148–158. https://doi.org/10.1016/j.conb.2014.07.009

Lynch, C. J., Elbau, I., & Liston, C. (2021). Improving precision functional mapping routines with multi-echo fMRI. *Current Opinion in Behavioral Sciences*, *40*, 113–119. https://doi.org/10.1016/j.cobeha.2021.03.017

Lynch, C. J., Power, J. D., Scult, M. A., Dubin, M., Gunning, F. M., & Liston, C. (2020). Rapid Precision Functional Mapping of Individuals using Multi-Echo fMRI. Cell Reports, 33(12). https://doi.org/10.1016/j.celrep.2020.108540

Madden, D. J., Jain, S., Monge, Z. A., Cook, A. D., Lee, A., Huang, H., Howard, C. M., & Cohen, J. R. (2020). Influence of structural and functional brain connectivity on age-related differences in fluid cognition. *Neurobiology of aging*, *96*, 205–222. https://doi.org/10.1016/j.neurobiolaging.2020.09.010

Malagurski, B., Liem, F., Oschwald, J., Mérillat, S., & Jäncke, L. (2020). Functional dedifferentiation of associative resting state networks in older adults – A longitudinal study. *NeuroImage*, *214*(February). https://doi.org/10.1016/j.neuroimage.2020.116680

Margulies, D. S., Ghosh, S. S., Goulas, A., Falkiewicz, M., Huntenburg, J. M., Langs, G., . . . Petrides, M. (2016). Situating the default-mode network along a principal gradient of macroscale cortical organization. Proceedings of the National Academy of Sciences, 113(44), 12574-12579.

McIntosh, A. R., & Lobaugh, N. J. (2004). Partial least squares analysis of neuroimaging data: Applications and advances. NeuroImage, 23, 250–263. https://doi.org/10.1016/j.neuroimage.2004.07.020

McIntosh, A.R., Mišić, B. (2013). Multivariate statistical analyses for neuroimaging data. Annual Review of Psychology, 64(1), 499–525. https://doi.org/10.1146/annurev- psych-113011- 143804.

Mwilambwe-Tshilobo, L., Ge, T., Chong, M., Ferguson, M. A., Misic, B., Burrow, A. L., … Spreng, R. N. (2019). Loneliness and meaning in life are reflected in the intrinsic network architecture of the brain. Social Cognitive and Affective Neuroscience, 14(4), 423–433. https://doi.org/10.1093/scan/nsz021

Mrvar, A., & Batagelj, V. (2016). Analysis and visualization of large networks with program package Pajek. *Complex Adaptive Systems Modeling*, *4*(1). https://doi.org/10.1186/s40294-016-0017-8

Murphy, A. C., Bertolero, M. A., Papadopoulos, L., Lydon‐Staley, D. M., & Bassett, D. S. (2020). Multimodal network dynamics underpinning working memory. *Nature Communications*, 11(1), 3035. https://doi.org/10.1038/s41467‐020‐15541‐0

Park, B.-y., Bethlehem, R. A., Paquola, C., Lariviere, S., Cruces, R. R., de Wael, R. V., . . . Bernhardt, B. (2020). Macroscale connectome manifold expansion in adolescence. bioRxiv. https://www.biorxiv.org/content/10.1101/2020.06.22.165621v2

Parkes, L., Fulcher, B., Yücel, M., & Fornito, A. (2018). An evaluation of the efficacy, reliability, and sensitivity of motion correction strategies for resting-state functional MRI. NeuroImage, 171(July 2017), 415–436. https://doi.org/10.1016/j.neuroimage.2017.12.073

Payer, D., Marshuetz, C., Sutton, B., Hebrank, A., Welsh, R. C., & Park, D. C. (2006). Decreased neural specialization in old adults on a working memory task. *Neuroreport*, *17*(5), 487–491. https://doi.org/10.1097/01.wnr.0000209005.40481.31

Power, J. D., Barnes, K. A., Snyder, A. Z., Schlaggar, B. L., & Petersen, S. E. (2012). Spurious but systematic correlations in functional connectivity MRI networks arise from subject motion. NeuroImage, 59(3), 2142–2154. https://doi.org/10.1016/j.neuroimage.2011.10.018

Power, J. D., Plitt, M., Gotts, S. J., Kundu, P., Voon, V., Bandettini, P. A., & Martin, A. (2018). Ridding fMRI data of motion-related influences: Removal of signals with distinct spatial and physical bases in multiecho data. *Proceedings of the National Academy of Sciences of the United States of America*, *115*(9), E2105–E2114. https://doi.org/10.1073/pnas.1720985115

Reitan, R. M. (1958). Validity of the Trail Making Test as an indicator of organic brain damage. *Perceptual and Motor Skills, 8,* 271–276. https://doi.org/10.2466/PMS.8.7.271-276

Saad, Z. S., Gotts, S. J., Murphy, K., Chen, G., Jo, H. J., Martin, A., & Cox, R. W. (2012). Trouble at rest: how correlation patterns and group differences become distorted after global signal regression. *Brain connectivity*, *2*(1), 25–32. https://doi.org/10.1089/brain.2012.0080

Saad, Z. S., Reynolds, R. C., Jo, H. J., Gotts, S. J., Chen, G., Martin, A., & Cox, R. W. (2013). Correcting brain-wide correlation differences in resting-state FMRI. *Brain connectivity*, *3*(4), 339–352. https://doi.org/10.1089/brain.2013.0156

Samanez-Larkin, G. R., & D'Esposito, M. (2008). Group comparisons: Imaging the aging brain. Social Cognitive and Affective Neuroscience, 3(3), 290–297. https://doi.org/10.1093/scan/nsn029

Schaefer, A., Kong, R., Gordon, E. M., Laumann, T. O., Zuo, X.-N., Holmes, A. J., … Yeo, B. T. T. (2018). Local-global parcellation of the human cerebral cortex from intrinsic functional connectivity MRI. Cerebral Cortex, 28, 3095–3114. https://doi.org/10.1093/cercor/bhx179

Shafiei, G., Zeighami, Y., Clark, C. A., Coull, J. T., Nagano-Saito, A., Leyton, M., ... & Mišić, B. (2019). Dopamine signaling modulates the stability and integration of intrinsic brain networks. *Cerebral Cortex*, *29*(1), 397-409.

Shipley, W. C., Gruber, C. P, Martin, T. A., & Klein, A. M. (2009). *Shipley-2 manual*. Los Angeles, CA: Western Psychological Services.

Smith, A. (1982). *Symbol Digit Modalities Test (SDMT) manual (revised)*.

Smith, S. M. (2002). Fast robust automated brain extraction. Human Brain Mapping, 17(3), 143–155. http://doi.org/10.1002/hbm.10062

Speck, O., Ernst, T., Chang, L., 2001. Biexponential modeling of multigradient-echo MRI data of the brain. Magn. Reson. Med. 45, 1116–1121. http://dx.doi.org/10.1002/ mrm.1147.

Spreng, R. N., Fernández-Cabello, S., Turner, G. R., & Stevens, W. D. (2019). Take a deep breath: Multiecho fMRI denoising effectively removes head motion artifacts, obviating the need for global signal regression. *Proceedings of the National Academy of Sciences of the United States of America*, *116*(39), 19241–19242. https://doi.org/10.1073/pnas.1909848116

Spreng, R. N., Stevens, W. D., Viviano, J. D., & Schacter, D. L. (2016). Attenuated anticorrelation between the default and dorsal attention networks with aging: evidence from task and rest. *Neurobiology of aging*, *45*, 149–160. https://doi.org/10.1016/j.neurobiolaging.2016.05.020

Spreng, R. N., & Turner, G. R. (2013). Structural covariance of the default network in healthy and pathological aging. *The Journal of Neuroscience : The Official Journal of the Society for Neuroscience*, *33*(38), 15226–15234. https://doi.org/10.1523/JNEUROSCI.2261-13.2013

Spreng, R. N., & Turner, G. R. (2019). The shifting architecture of cognition and brain function in older adulthood. *Perspectives on Psychological Science*. Retrieved from http://citeseerx.ist.psu.edu/viewdoc/download?doi=10.1.1.169.5067&rep=rep1&type=pdf

Stevens, W. D., & Spreng, R. N. (2014). Resting-state functional connectivity MRI reveals active processes central to cognition. *Wiley Interdisciplinary Reviews: Cognitive Science*, *5*(2), 233–245. https://doi.org/10.1002/wcs.1275

Stumme, J., Jockwitz, C., Hoffstaedter, F., Amunts, K., & Caspers, S. (2020). Functional network reorganization in older adults: Graph-theoretical analyses of age, cognition and sex. *NeuroImage*, *214*(February). https://doi.org/10.1016/j.neuroimage.2020.116756

Sullivan, M. D., Anderson, J., Turner, G. R., Spreng, R. N., & Alzheimer's Disease Neuroimaging Initiative (2019). Intrinsic neurocognitive network connectivity differences between normal aging and mild cognitive impairment are associated with cognitive status and age. *Neurobiology of aging*, *73*, 219–228. https://doi.org/10.1016/j.neurobiolaging.2018.10.001

Tsvetanov, K. A., Henson, R. N. A., Jones, P. S., Mutsaerts, H., Fuhrmann, D., Tyler, L. K., & Rowe, J. B. (2020). The effects of age on resting-state BOLD signal variability is explained

by cardiovascular and cerebrovascular factors. *Psychophysiology*, (September 2019), 1–20. https://doi.org/10.1111/psyp.13714

Turner, G., & D'Esposito, M. (2014). Neurorehabilitation of executive functions. In M. Selzer, S. Clarke, L. Cohen, G. Kwakkel, & R. Miller (Eds.), *Textbook of Neural Repair and Rehabilitation* (pp. 489-499). Cambridge: Cambridge University Press. doi:10.1017/CBO9780511995590.042

Vos de Wael, R., Benkarim, O., Paquola, C. et al. BrainSpace: a toolbox for the analysis of macroscale gradients in neuroimaging and connectomics datasets. Commun Biol 3, 103 (2020). https://doi.org/10.1038/s42003-020-0794-7

Wang, D., Buckner, R. L., Fox, M. D., Holt, D. J., Holmes, A. J., Stoecklein, S., Langs, G., Pan, R., Qian, T., Li, K., Baker, J. T., Stufflebeam, S. M., Wang, K., Wang, X., Hong, B., & Liu, H. (2015). Parcellating cortical functional networks in individuals. *Nature neuroscience*, *18*(12), 1853–1860. https://doi.org/10.1038/nn.4164

Wechsler, D. (2009). *Wechsler Memory Scale (Fourth Edition)*. San Antonio, TX: Pearson.

Worsley, K.J., Taylor JE, Carbonell F, Chung MK, Duerden E, Bernhardt B, Lyttelton O, Boucher M, Evans (2009). SurfStat: A Matlab toolbox for the statistical analysis of univariate and multivariate surface and volumetric data using linear mixed effects models and random field theory. *NeuroImage*, 47, Supplement 1, S102, https://doi.org/10.1016/S1053-8119(09)70882-1.

Yeo, B. T. T., Kirienen, F. M., Sepulcre, J., Sabuncu, M. R., Lashkari, D., Hollinshead, M., . . . Buckner, R. L. (2011). The organization of the human cerebral cortex estimated by intrinsic functional connectivity. J Neurophysiol, 106, 1125-1165. doi:10.1152/jn.00338.2011.

Yesavage, J. A., & Brink, T. L. (1983). Development and validation of geriatric depression screening scale: A preliminary report. Journal of Psychiatric Research, 80(1), 37–49. http://doi.org/10.2307/1957152

Zelazo, P. D., & Carlson, S. M. (2012). Hot and cool executive function in childhood and adolescence: Development and plasticity. *Child Development Perspectives, 6*(4), 354–360.

Zonneveld, H. I., Pruim, R. H., Bos, D., Vrooman, H. A., Muetzel, R. L., Hofman, A., … Vernooij, M. W. (2019). Patterns of functional connectivity in an aging population: The Rotterdam Study. *NeuroImage*, *189*(January), 432–444. https://doi.org/10.1016/j.neuroimage.2019.01.041

Supplemental Material

Supplementary Figure 1

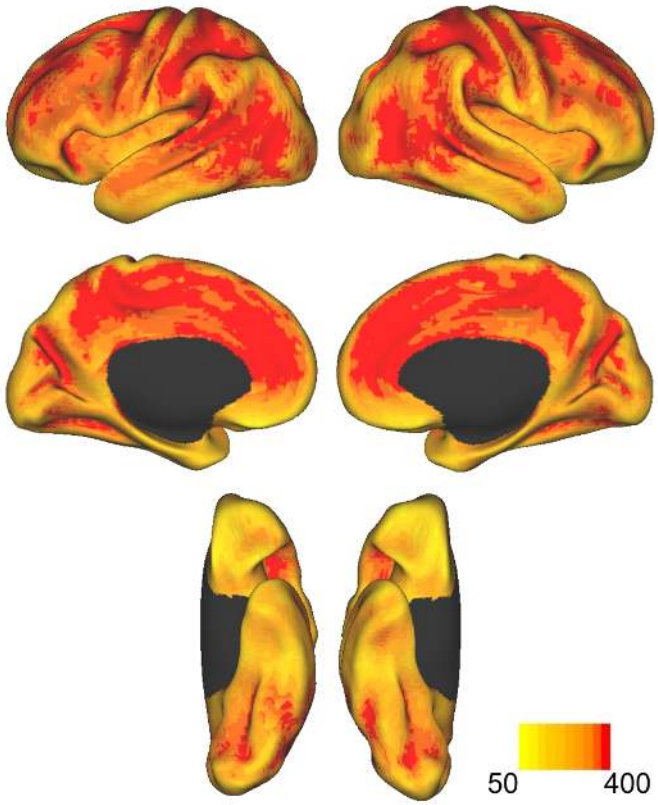

Supplementary Figure 1 Caption: Temporal Signal to Noise. A temporal signal to noise ratio (tSNR) map was created for both runs of each participant's denoised data and averaged. The average group map (N=301) was projected onto an inflated surface, separated by L and R hemispheres. Maps were thresholded to demonstrate that the low end of tSNR values were well above 50. A maximum tSNR of 400 is shown here for visualization purposes.

Supplementary Figure 2

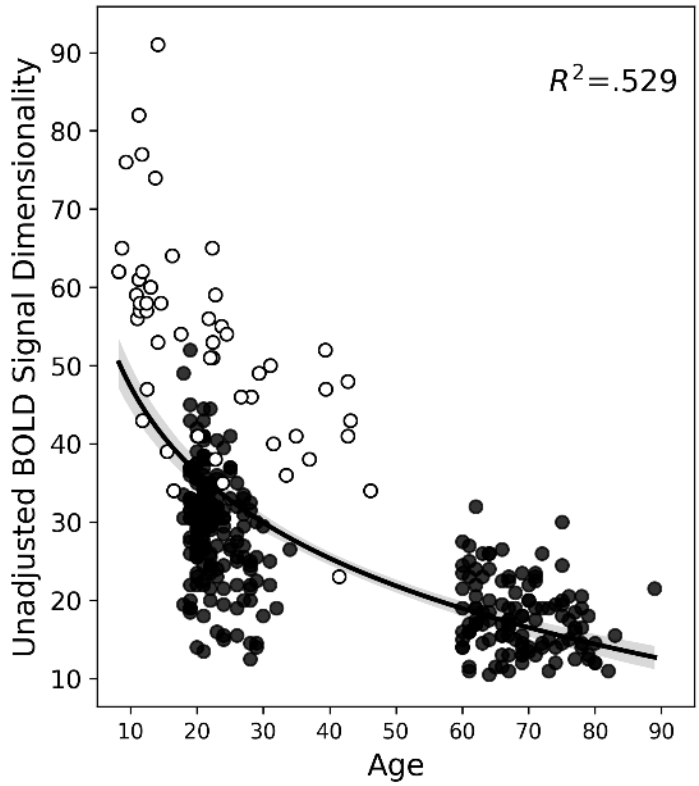

Supplementary Figure 2 Caption: BOLD signal dimensionality. The scatter plot shows BOLD signal dimensionality by age with a power distribution and 95% confidence intervals overlaid. Points in white were contributed by Kundu and colleagues (2018). Here, BOLD dimensionality is not adjusted by number of time points acquired. BOLD dimensionality was averaged across two runs for points in black.

Supplementary Figure 3

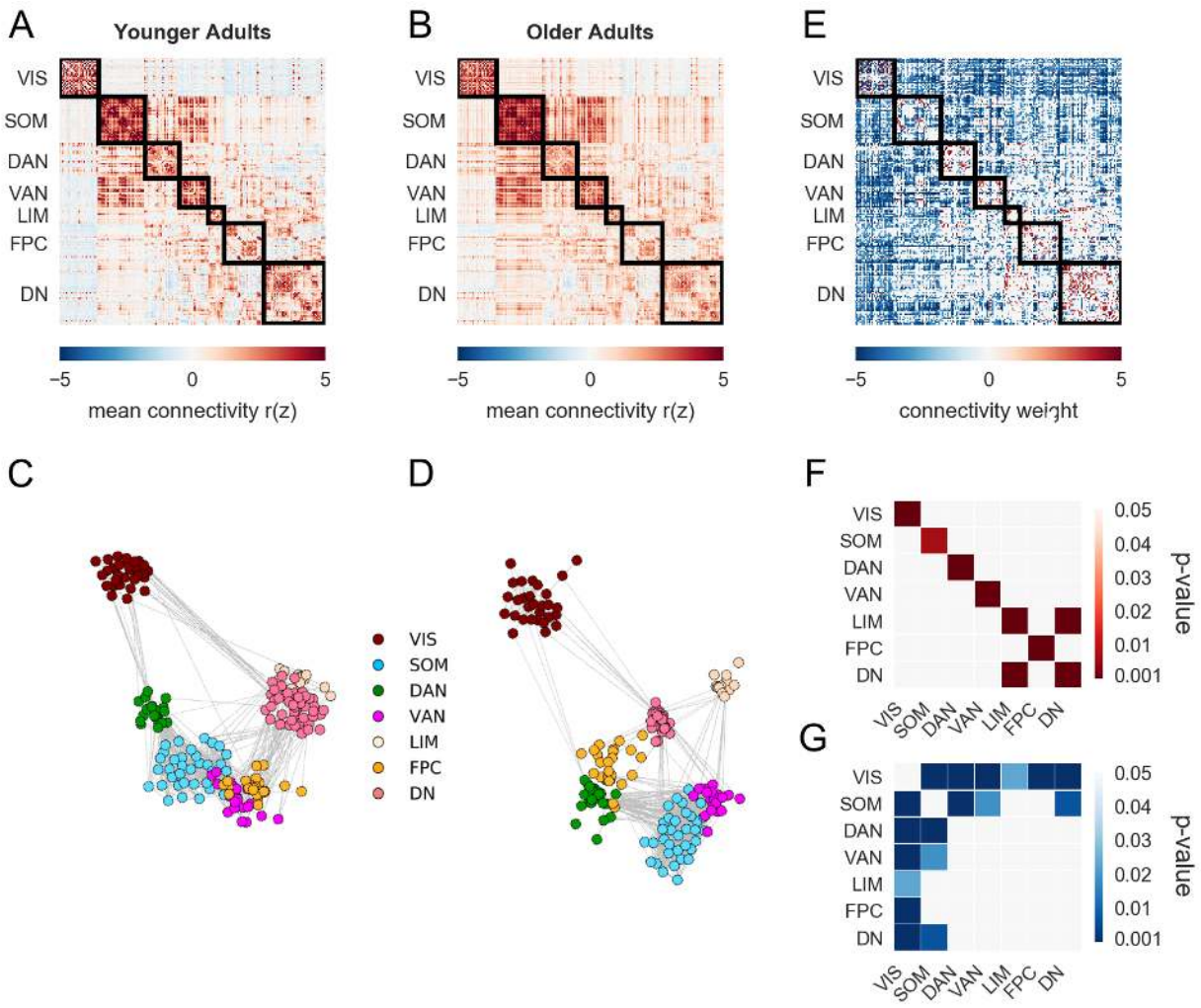

Supplementary Figure 3 Caption: Functional connectomics in younger and older adults. Mean RSFC for the 200-parcellated MEFC data in (A) younger and (B) older adults. Spring-embedded plots with a 7-network solution (5% edge density) of the mean correlation matrices for (C) younger and (D) older adults. (E) Multivariate PLS analysis was used to identify age-related differences in RSFC between younger and older adults. Red color indicates greater RSFC in younger adults, and blue color indicates greater RSFC in older adults. (F-G) Network contributions reflecting differences in large-scale distributed networks. (F) Greater within- and between- network connectivity in young, lower in older adults. (G) Greater within- and between- network connectivity in older adults, lower in younger adults. The mean positive (F) and negative (G) bootstrap ratios within and between networks are expressed as a p-value for each z-score relative to a permuted null model. Higher values indicate greater connectivity than predicted by the null distribution. VIS = visual, SOM= somatomotor, DAN= dorsal attention, VAN = ventral attention, LIM = limbic, FPC= frontoparietal control, DN= default.

Supplementary Figure 4

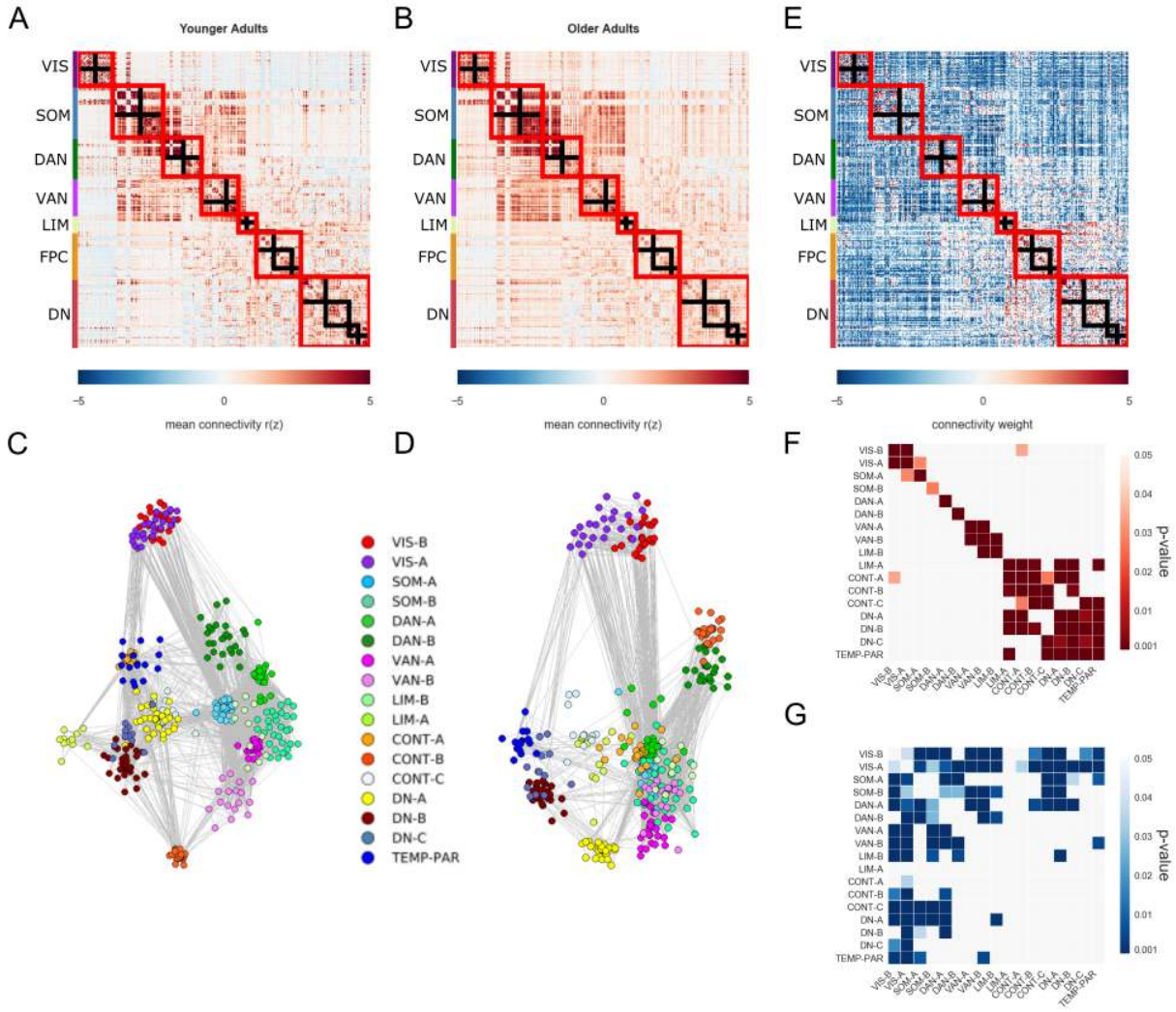

Supplementary Figure 4 Caption: Functional connectomics in younger and older adults. Mean RSFC for the 400-parcellated MEFC data in (A) younger and (B) older adults. Spring-embedded plots with a 17-network solution (5% edge density) of the mean correlation matrices for (C) younger and (D) older adults. (E) Multivariate PLS analysis was used to identify age-related differences in RSFC between younger and older adults. Red color indicates greater RSFC in younger adults, and blue color indicates greater RSFC in older adults ($p<0.0001$; 100% variance explained). (F-G) Network contributions reflecting differences in large-scale distributed networks. (F) Greater within- and between- network connectivity in young, lower in older adults. (G) Greater within- and between-network connectivity in older adults, lower in younger adults. The mean positive (F) and negative (G) bootstrap ratios within and between networks are expressed as a p-value for each z-score relative to a permuted null model. Higher values indicate greater connectivity than predicted by the null distribution. VIS = visual, SOM= somatomotor, DAN= dorsal attention, VAN = ventral attention, LIM = limbic, FPC= frontoparietal control, DN= default.

Supplementary Figure 5

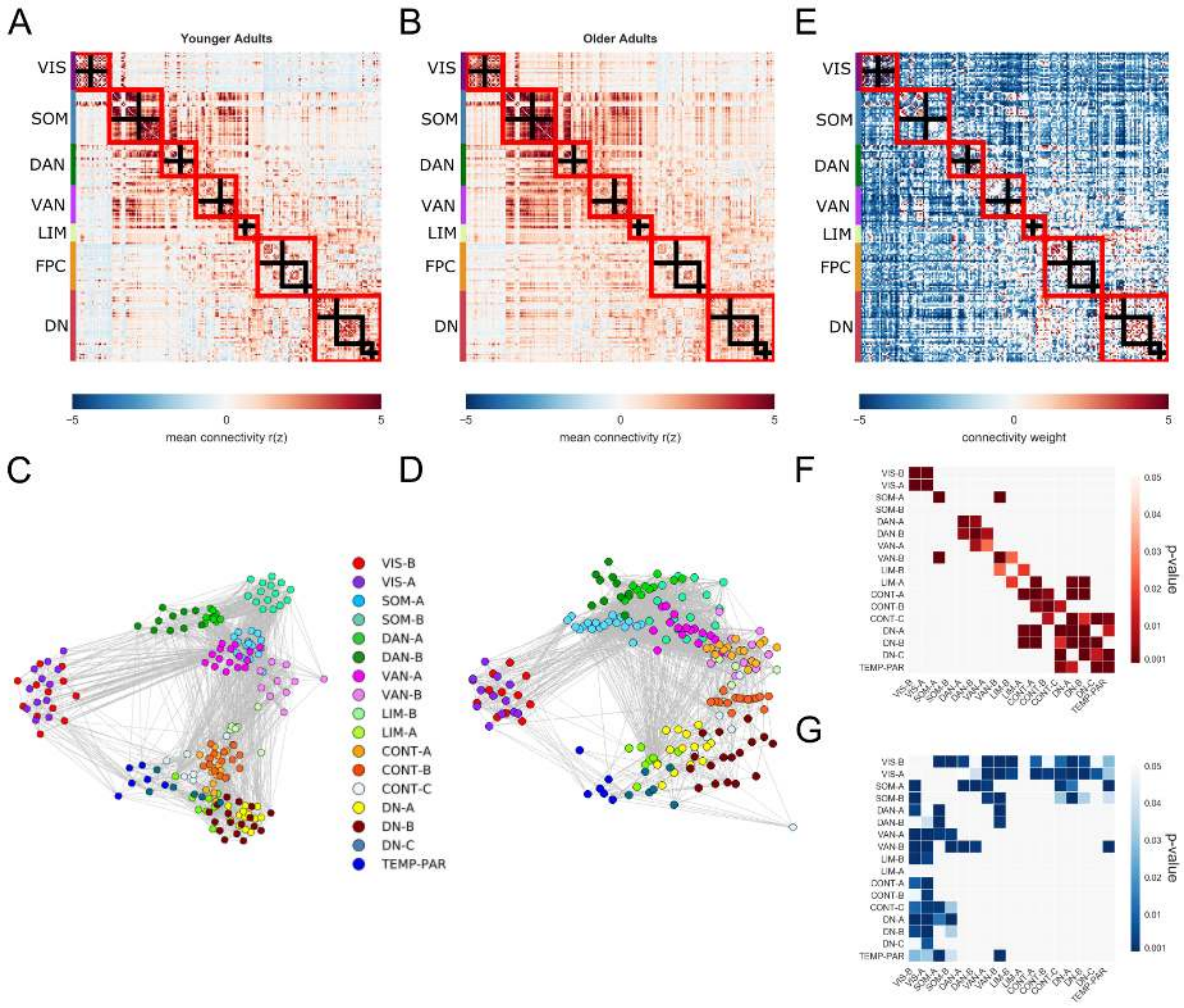

Supplementary Figure 5 Caption: Functional connectomics in younger and older adults. Mean RSFC for the 200-parcellated MEFC data in (A) younger and (B) older adults. Spring-embedded plots with a 17-network solution (10% edge density) of the mean correlation matrices of (C) younger and (D) older adults. The threshold used for the spring-embedded plots was set at a higher threshold due to the sparsity of the graph at thresholds lower than 10%. (E) Multivariate PLS analysis was used to identify age-related differences in RSFC between younger and older adults ($p<0.0001$; 100% variance explained). Red color indicates greater RSFC in younger adults, and blue color indicates greater RSFC in older adults. Network contributions reflecting differences in large-scale distributed networks between (F) younger and (G) older adults. The mean positive bootstrap ratios within and between networks are expressed as a z-score relative to a permuted null model. Higher values indicate greater than expected connectivity in both age groups. VIS = visual; SOM=somatomotor; DAN= dorsal attention; VAN = ventral attention; LIM = limbic, FPC= frontoparietal control, DN= default.

Supplementary Figure 6

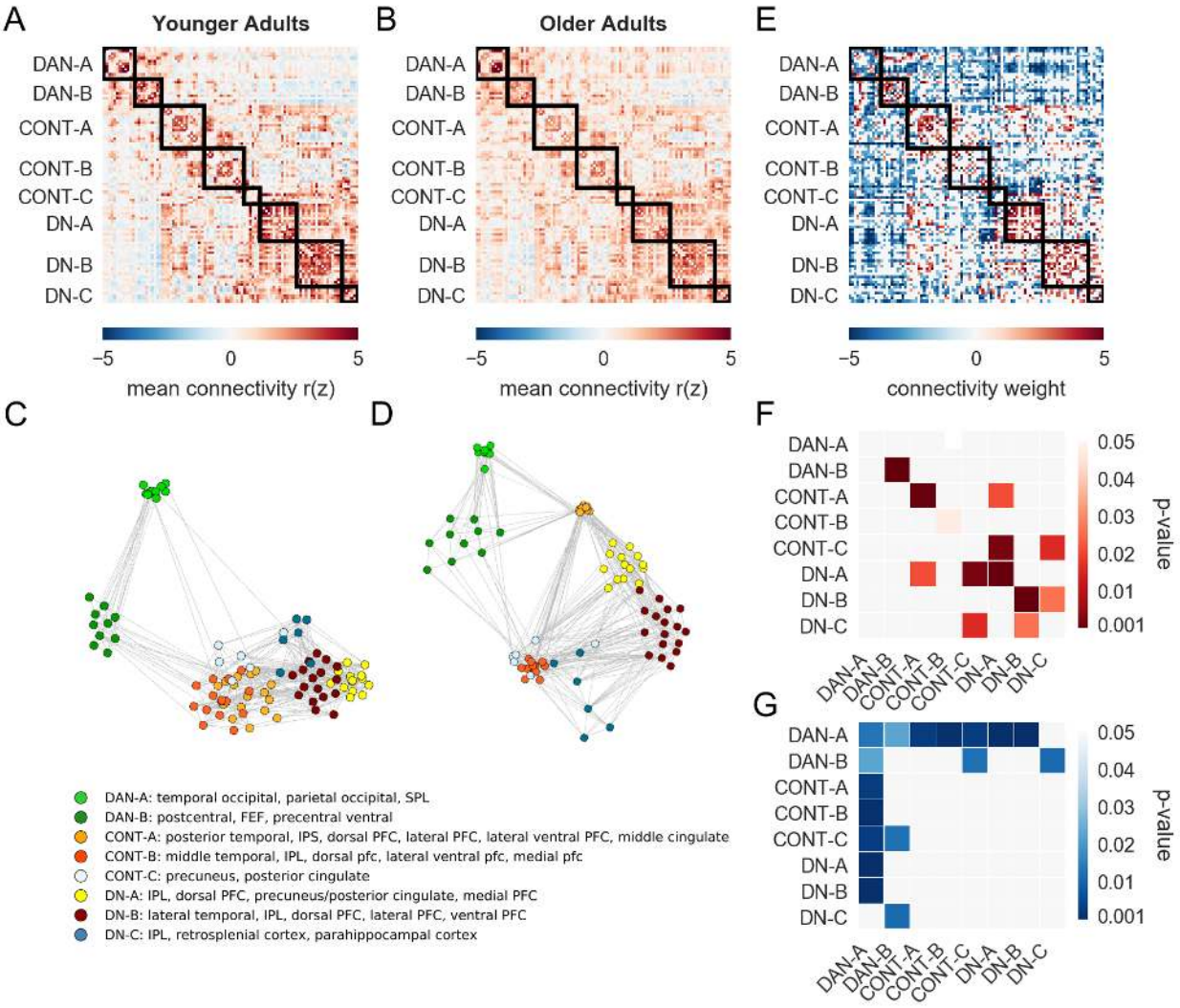

Supplementary Figure 6 Caption: Functional connectivity of the dorsal attention (DAN), frontoparietal control (CONT), and default (DN) sub-networks following Yeo 17-network solution. Mean group connectivity for the 200-parcellated MEFC data in (A) younger and (B) older adults. Spring-embedded plots (10% edge density) of the mean correlation matrices for (C) younger and (D) older adults. A lower threshold was used for the spring-embedded plots due to the sparsity of the graph at higher thresholds ($p<0.0001$;100% variance explained). (E) Differences in RSFC between younger and older adults among DAN, CONT, and DN. (F) Greater within- and between- network connectivity in young. (G) Greater within- and between- network connectivity in older adults.

Supplementary Figure 7

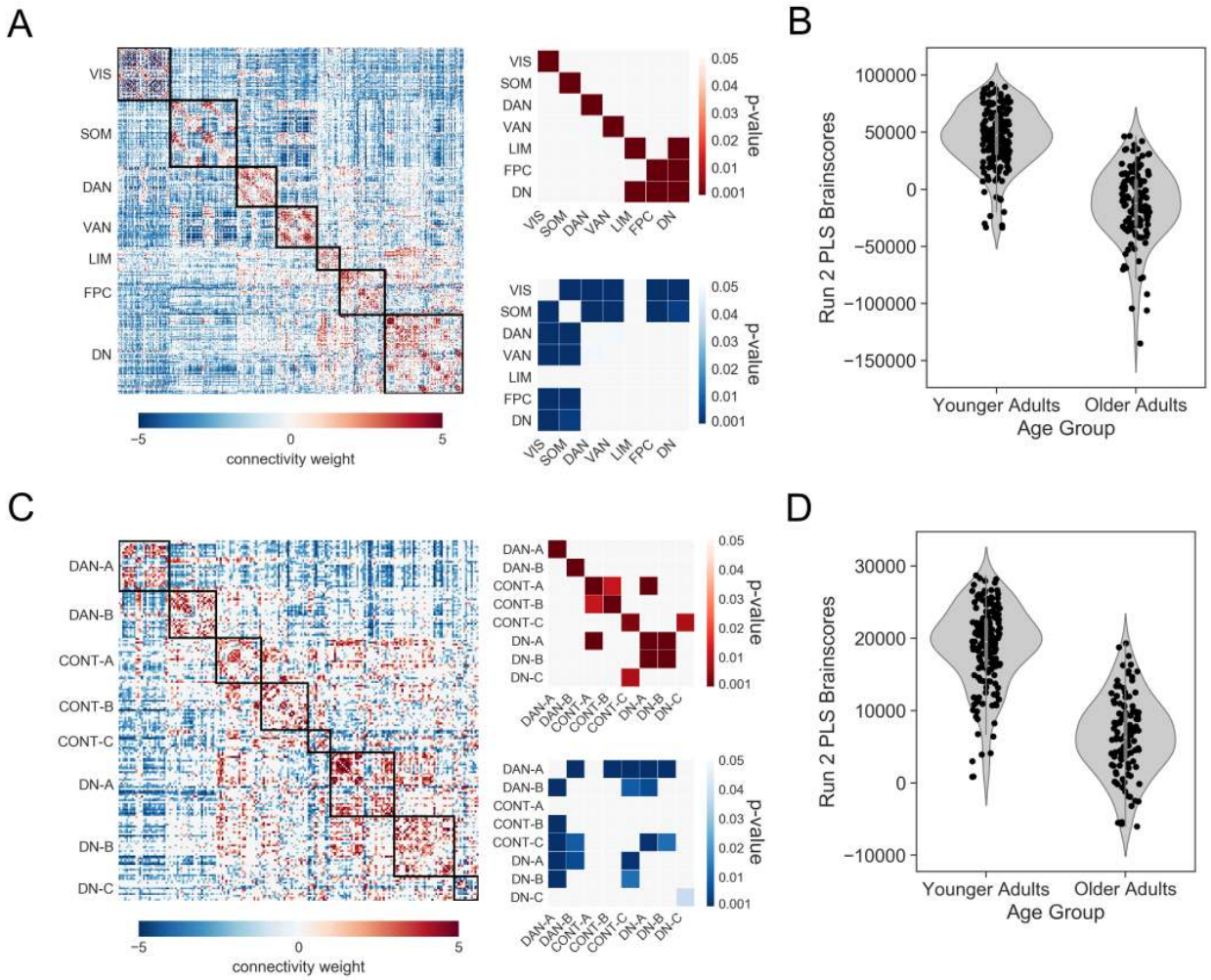

Supplementary Figure 7 Caption: Cross-validation of the PLS results. (A) Age differences in the full functional connectome from run one. (B) Group differences in brain scores computed from run two, based upon the edge-weights determined in run one. (C) Age differences in the functional connectivity of the dorsal attention (DAN), frontoparietal control (CONT), and default (DN) sub-networks from run one. (D) Group differences in brain scores computed from run two, based upon the edge-weights determined in run one.